2

Drift ice material

2.1 SEA ICE COVER

This chapter presents the material structure of sea ice from local scale to large scale. Ice floes form granular drift ice fields, for which continuum approximations are used when the scale of interest is much larger than the floe size. These fields are characterized by their ice type, ice compactness, floe size and shape, and ice thickness, as shown in Sections 2.1 and 2.2. Section 2.3 is devoted to thermodynamics of sea ice, which is closely coupled with dynamics and which is a necessary element in sea ice dynamics models. Section 2.4 presents the ice thickness distribution, and Section 2.5 deals with ice ridges, the thickest accumulations of mechanically deformed ice, which have a key role in the mechanical energy budget of drift ice. The chapter ends with Section 2.6 introducing the concept of "ice state" – a set of material properties of drift ice necessary to understand and model its dynamics.

In the world sea ice cover, ice occurs all year in the *perennial sea ice zone*, covering the inner Arctic Ocean north of about 80°N and smaller sections in the Antarctica, mainly the western Weddell Sea. Ice occurs only in winter in an area called the *seasonal sea ice zone* (SSIZ), extending on average down to 60° latitudes.

Table 2.1 and Figure 2.1 show the main sea ice basins, with sizes ranging from 200 km to 3000 km. Southern Ocean sea ice cover is actually a ring, 20,000 km long and with a width ranging from almost zero in summer to 1000 km in winter, centred around Antarctica at 60–70°S. Within freezing seas there are smaller sub-basins, which contain dynamically independent ice packs such as the Gulf of Riga in the Baltic Sea (size $L = 100$ km and typical ice thickness $h = 0.2$ m). The drift ice basin closest to the equator is the Bo Hai Sea (Gulf of Chihli) off the coast of China, located between the latitudes of 37° and 41°N[1].

[1] Sea ice forms occasionally in the Chesapeake Bay estuary on the east coast of USA at similar latitudes but drift ice phenomena are not of concern there.

M. Leppäranta, *The Drift of Sea Ice*, Springer Praxis Books,
DOI 10.1007/978-3-642-04683-4_2, © Springer-Verlag Berlin Heidelberg 2011

Nikolai Nikolaevich Zubov (1885–1960), a great pioneer in the science of sea ice, its physics and its geography. He was the author of the monumental book *L'dy Arktiki [Arctic Ice],* published in 1945 in Moscow and translated into English in 1963.
Reproduced from Collections of the Russian State Museum of Arctic and Antarctic, St. Petersburg, with permission.

The thickness of ice is 2–5 m in the Arctic Ocean and Greenland Sea, while in the SSIZ it is an order of magnitude less. For an enclosed drift ice basin there is no ice exchange with neighbouring seas, while in an open basin a large part of the ice boundary is toward open water and the mobility of the ice is therefore greater. The ratio $\delta = h/L$, which characterizes the stability of a solid ice sheet in a basin, ranges from 10^{-7} to 5×10^{-6} in sea ice basins where drift ice occurs (Table 2.1). In subarctic medium size lakes ($L \sim 10$ km, $h \sim 0.5$ m), $\delta \sim 5 \times 10^{-5}$, and the ice forms a solid stationary sheet. In Lake Ladoga, the largest lake in Europe, we have $L = 100$ km and $h = 0.5$ m and the ice cover is mobile as suggested by $\delta = 5 \times 10^{-6}$.

2.1.1 Sea ice landscape

A "sea ice landscape" consists of leads and ice floes with ridges, hummocks, and other variable morphological characteristics. *Ice types* have been defined to provide practical standards for observers (WMO, 1970; see also `http://www.aari.nw.ru/` for updates). They originate from shipping activities in ice-covered waters

Table 2.1 The main basins of the world ocean's ice zone. The types, E = enclosed, SE = semi-enclosed and O = open, refer to the ice exchange with neighbouring seas.

Basin	Size L (km)	Type	Ice thickness, h (m)	Stability, h/L ($\times 10^{-6}$)
Central Arctic	3000	SE	2–5	0.7–2
Greenland Sea	1000	O	2–5	2–5
Barents Sea	1000	O	1–2	1–2
Kara Sea	1000	SE	1–2	1–2
White Sea	200	SE	0.1–1	0.5–5
Baltic Sea	500	E	0.1–1	0.2–2
Sea of Azov	200	E	0.1–0.2	0.5–1
Sea of Okhotsk	1000	SE	0.1–2	0.2–4
Bohai Sea	300	E	0.1–0.3	0.3–1.0
Bering Sea	1000	SE	0.1–1	0.1–1
Hudson Bay	500	E	0.5–1	1–2
Gulf of St Lawrence	300	E	0.1–1	0.3–3
Labrador Sea	500	O	0.5–1	1–2
Baffin Bay	500	SE	1–2	2–4
Southern Ocean	1000	O	0.5–2	0.5–2
Weddell Sea	1500	O	0.5–3	0.3–2
Ross Sea	500	O	0.5–1	1–2

and are based on appearance (i.e., how the ice looks to an observer on a ship or in an aircraft: Figures 2.2 and 1.2). This ice-type classification system has worked fairly well and has not suffered from severe subjective biases. The formation mechanism, aging, and deformation influence the appearance. Thus appearance provides information of ice thickness, which is seldom known from direct measurements. Some ice-type names are based on their resemblance to familiar objects (Figure 2.3).

Definitions

Let us now give a brief list of the necessary sea ice nomenclature for dynamics based on internationally agreed standards (Armstrong *et al.*, 1966; WMO, 1970):

Ice in the ocean

- *Sea ice*. Any form of ice found at sea that originates from the freezing of seawater.
- *Ice of land origin*. Ice formed on land or in an ice shelf, found floating in water.

Age of ice

- *New ice*. A general term for recently formed ice.
  - *Frazil ice*. Fine spicules or plates of ice suspended in water.
  - *Nilas*. A thin, elastic crust of ice that easily bends under the action of waves and swell and rafts under pressure (matt surface and thickness up to 10 cm).

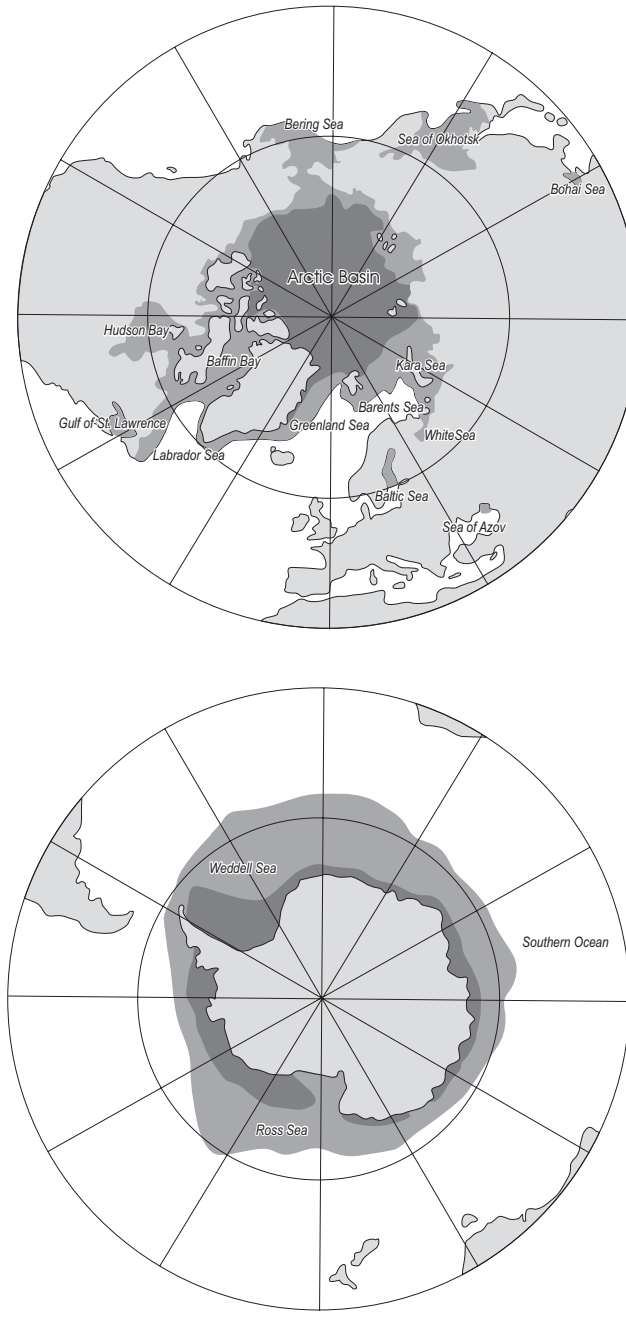

Figure 2.1 The world sea's ice zones in summer and winter. Dark area shows the perennial ice, lighter area shows the seasonal sea ice zone.
From Untersteiner (1984), with modifications for subarctic small basins.

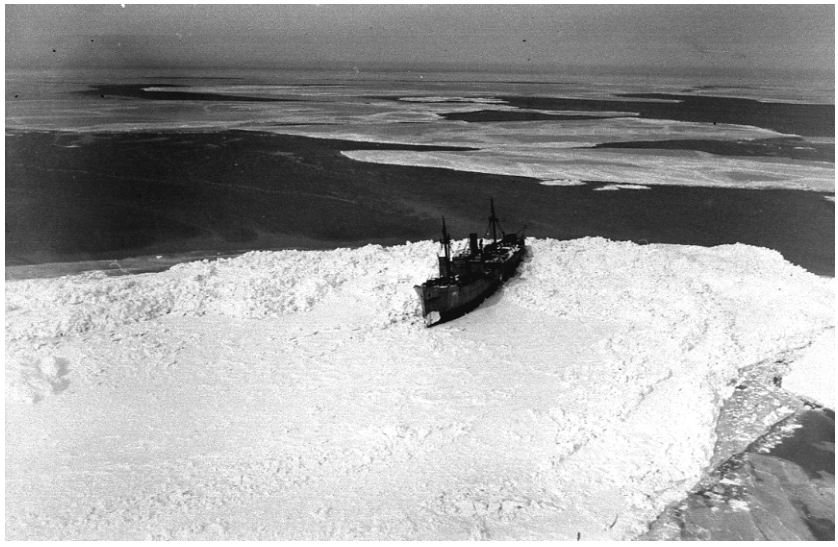

Figure 2.2 Aerial photograph from a Finnish Air Force ice reconnaissance flight in the Central Baltic, winter 1942. Airborne reconnaissance meant a huge step in understanding the morphology and drift of sea ice. The pilot was Erkki Palosuo, who later became a sea ice geophysicist and used his sea ice data from the Second World War for his doctoral thesis (Palosuo, 1953).
Reproduced with permission from Erkki Palosuo.

Figure 2.3 Pancake ice (the ice pieces shown are about 1 m across), also named lotus ice in the Far East, blini ice in Russia, and plate ice in Scandinavia and Finland.

- *Young ice*. Ice in transition between new ice and first-year ice (10–30 cm thick).
- *First-year ice*. Ice with no more than 1 year's growth that develops from young ice (thickness 30 cm to 2 m). Level when undeformed, but where ridges and hummocks occur, it is rough and sharply angular.
- *Multi-year ice*. Ice of more than 1 year's growth (thickness over 2 m). Hummocks and ridges are smooth and the ice is almost salt-free.

Forms of ice

- *Landfast ice*. Sea ice that remains fast along the coast, over shoals, or between grounded icebergs (also called *fast ice*).
- *Grounded ice*. Floating ice that finds itself aground in shoal water.
- *Drift ice*. Term used in a wide sense to include any sea ice other than fast ice (a substitute term is *pack ice*).
- *Ice field*. Area of drift ice at least 10 km across.
- *Pancake ice*. Pieces of new ice, usually approximately circular, about 30 cm to 3 m across and with raised rims due to the pieces striking against each other.
- *Ice floe*. Any relatively flat piece of ice 20 m or more across.
- *Level ice*. Sea ice that is unaffected by deformation (a substitute term is *undeformed ice*).
- *Deformed ice*. A general term for ice that has been squeezed together and in places forced upward and downward (a substitute term is *pressure ice*).
- *Rafted ice*. A form of pressure ice in which one floe overrides another. A type of rafting common in nilas whereby interlocking thrusts are formed – each floe thrusting "fingers" alternatively over and under the other – is known as *finger rafting*.
- *Brash ice*. Accumulations of ice made up of fragments no more than 2 m across (the wreckage of other forms of ice).
- *Hummocked ice*. A form of pressure ice in which pieces of ice are piled haphazardly, one piece over another, to form an uneven surface.
- *Ridge*. A ridge or wall of broken ice forced up by pressure (the upper – above water level – part is called the *sail* and the lower part the *keel*).

Openings in ice cover

- *Ice compactness*. The amount of sea surface covered by ice as a fraction of the whole area being considered (a substitute term is *ice concentration*).
- *Crack*. Any fracture that has not parted more than 1 metre.
- *Fracture*. Any break or rupture in ice resulting from deformation processes (length from metres to kilometres).
- *Lead*. Any fracture or passageway through sea ice that is navigable by surface vessels. Leads are opened by wind or ocean current forcing.
- *Polynya*. Any nonlinear-shaped opening enclosed in ice. Typical forms are *coastal polynyas* driven by persistent offshore winds and *open ocean polynyas* driven largely by upwelling of warm deeper water.
- *Ice edge*. The demarcation between the open sea and sea ice.

Table 2.2 Classification of ice concentration A (WMO, 1970).

Verbal	Numerical	Verbal	Numerical
Ice free	$A = 0\%$	Very open drift ice	$0\% < A < 30\%$
Open drift ice	$30\% \leq A < 50\%$	Close drift ice	$50\% \leq A < 70\%$
Very close drift ice	$70\% \leq A < 90\%$	Compact drift ice	$90\% \leq A \leq 100\%$

Ice compactness or *ice concentration*, denoted by A, is normally given in percentages or tenths and further categorised into six standard classes (Table 2.2; Figure 2.4). Between ice and open water surfaces, apart from melting conditions, there are strong contrasts and satellite remote sensing methods can detect them. Ice compactness is a key dynamic state variable as it tells of the mobility of drift ice fields.

The polar oceans also contain ice of land origin. By the mechanism called *calving*, pieces of ice break away from land ice masses facing the ocean. These pieces are classified (WMO, 1970) according to their size: *icebergs* (top more than 5 m above sea level), *ice islands* (top about 5 m above sea level and area more than few thousand square metres), *bergy bits* (top 1–5 m above sea level and area 100–300 m^2), and *growlers* (smaller than bergy bits). These pieces differ from sea ice floes by their ice quality (fresh water ice), thickness and three-dimensional character.

2.1.2 Sea ice zones

In a given basin, sea ice cover can be divided into zones of different dynamic character (Weeks, 1980): central pack, shear zone, landfast ice, and marginal ice zone. Shear zone and landfast ice form the coastal boundary zone, while the marginal ice zone is the boundary zone toward the open ocean. Very small basins only contain fast ice and the width of the boundary zones – marginal ice zone and shear zone – is of the order of 100 km.

The central pack consists of the interior ice that is free from immediate influence from the boundaries. Changes are smoother there than in the boundary zones and are caused by external forcing. The length scale is the size of the basin itself; but due to the width of boundary zones, the central pack only exists in large seas.

Landfast ice, or *fast* ice, is the immobile coastal sea ice zone, stationary for most of the ice season. The width of this zone depends on the thickness of ice, topography of the sea bottom, and the areal density of islands and grounded forms of ice. Fast ice extent develops stepwise, in an almost discontinuous manner (Jurva, 1937; Divine, 2003). Grounding of sea ice ridges creates fixed support points to stabilize the ice sheet. Because of the size of ridges and ice thickness, in Arctic seas the fast ice zone extends to depths of about 10–20 m (Zubov, 1945; Volkov *et al.*, 2002) while in subarctic seas such as the Baltic Sea the limit is normally close to 10 m (Leppäranta, 1981b). In Antarctic waters, grounded icebergs may act as tie points for fast ice

formation, and therefore the fast ice zone may extend deeper into the ocean as well (e.g., Massom *et al.*, 2003). Off Hokkaido in the Sea of Okhotsk, there are no islands and the depth of the sea increases rapidly with distance from the shoreline. Tides "clean" the ice that forms close to the shore, and as a consequence the fast ice zone is practically non-existent.

The shear zone is the boundary zone of the drift ice field next to the landfast ice (or coast). There the mobility of the ice is restricted by the geometry of the boundary and strong deformation takes place. The width is 10–200 km. A well-developed shear zone is found on the coast of the Beaufort Sea of the Arctic Ocean. Based on deformation data, Hibler *et al.* (1974a) concluded its representative width was around 50 km. At the solid boundary, ice velocity is sensitive to the forcing direction (Goldstein *et al.*, 2009). The velocity is often discontinuous across the boundary, thus modifying local hydrography and circulation. In basins of $\sim$100 km length scale, such as the Bay of Bothnia in the Baltic Sea, the whole ice pack feels the presence of land, and geometric steering by the basin is seen in ice motion.

The marginal ice zone (MIZ) lies along the boundary of open water and sea ice cover. It is loosely characterized as the area of pack ice where the influence of the open ocean is directly observed. MIZ extends to a distance of 100 km from the ice edge (Wadhams, 1980b; Squire, 1998). This distance corresponds to the penetration distance of ocean swell into a drift ice field; this distance also corresponds to the length scale below which the wind fetch over ice is not long enough to build ice ridges. In the MIZ, there is a large temporal and spatial variability of ice conditions and intensive air–ice–sea interaction. Off-ice winds cause MIZ diffusion, while on-ice winds drive the ice to form a sharply compact ice edge (Zubov, 1945). The open sea influence is strongest in a narrow *ice edge zone*, width up to 5 km.

Well-developed MIZs are found along the oceanic ice edge of the polar oceans, and their locations are largely controlled by the polar fronts. At a compact ice edge there is a discontinuity in sea surface velocity and roughness, and possibly a front in temperature and salinity. They affect the mesoscale circulation in the ocean, resulting in eddies and jets as well as ice edge upwelling and downwelling. A front may also form in the atmospheric boundary layer. In smaller, subarctic seas there is usually not time enough for a proper marginal ice zone to develop. In such seas, ice cover extends and retreats a long distance back and forth during a short ice season. Ice edge zones, however, develop quickly and are a common feature at the ice margin under on-ice wind forcing.

In the past, the ice margin used to be considered the border of an unknown ocean where the ice mysteriously transported sand and driftwood from unknown places. And as such drifting sea ice was strange, it inspired the Vikings to name a new land – Iceland – due to the presence of drift ice in its fjords.

2.1.3 Sea ice charting

Sea ice charting began in the late 1800s for navigation in ice-covered waters. Due to the dynamics of sea ice, the charts need daily updating and therefore much is

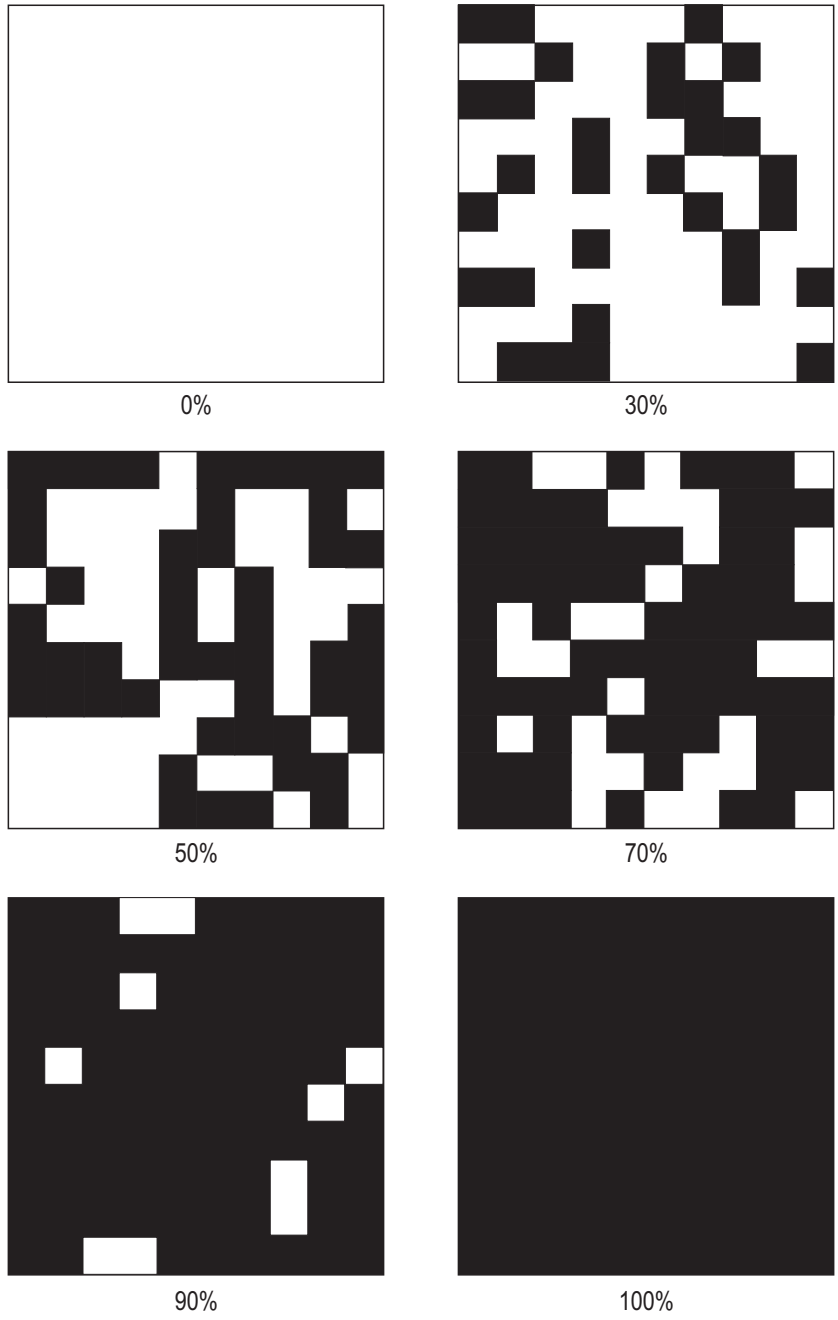

Figure 2.4 Classification of ice concentration (WMO, 1970), with the class boundaries illustrated by random binary charts. From left up to right down: open water, very open drift ice, open drift ice, close drift ice, very close drift ice, compact drift ice.

required of the mapping methods. Before the time of airborne and spaceborne remote sensing, ice charts were based on ship reports and occasional ground truth observations, which provide only limited information. Aerial reconnaissance played an important role until the 1970s, but since then satellite observation technology has been the main method of data collection. Sea ice information is presented according to an international standard (WMO, 2000). However, ships operating in ice conditions also take original satellite images to see detailed ice conditions along a planned route.

Polar orbiting weather satellites, such as the *NOAA AVHRR* series, with optical and infrared channels were taken into ice charting in the 1970s. However, both channels are limited by cloudiness, and the optical channel is further limited by the lack of sunlight in polar winter. Due to the weather limitations, microwave methods have become a critically important complementary tool. Soviet Union *Okean* series satellites produced simultaneous optical–radar image pairs for ice conditions in the Northern Sea Route in the 1980s (e.g., Johannessen *et al.*, 2006). At present, passive microwave mapping is the principal method for regular, global sea ice charting, mainly using US Defense Meteorological Satellite Program (DMSP) special sensor microwave imager (SSM/I) data (Figure 2.5), available via the National Snow and Ice Data Center (NSIDC) in Boulder, Colorado (`http://nsidc.org`) (Cavalieri *et al.*, 1999). This method is weather- and light-independent but limited by low spatial resolution (20–30 km), too small for regional ice charting.

Synthetic aperture radar (SAR) has become an extremely useful complementary tool. The first extensive satellite SAR data set was collected by *ERS-1*, launched by the European Space Agency (ESA) in 1991. A few years later, the *Radarsat* satellite series was started in Canada, commercial satellites designed for sea ice mapping (Stern and Moritz, 2002; Belchansky and Douglas, 2002; `http://www.radarsat2.info/`). SAR technique provides high spatial resolution but has limitations. A balance must be chosen between repeat cycle, swath and spatial resolution (i.e., full coverage of an area is possible with 5-day repeat cycles using lower resolution). Also, interpretation of the radar signal for sea ice information is sometimes problematic. Ice conditions change significantly on a daily basis in the seasonal sea ice zone (Leppäranta, 1981a; Leppäranta *et al.*, 1998), and the relation between sea ice and radar image is not one-to-one (Carsey, 1992; Wadhams, 2000). For example, ice and open water signatures are not always different, and ridges may be mixed with frost flowers on thin ice in narrow leads. Radar is at its best, in mapping ice kinematics.

An example of a sea ice chart over the Arctic is given in Figure 2.6. Ice charts basically present ice compactness and ice type. In subarctic seas with heavy winter traffic, ice charts are invaluable in providing information about the ice thickness and floe size. In the Baltic Sea, each of the nine coastline countries has an ice service for regional ice charting (e.g., `http://www.fmi.fi/weather/index_9.html/` for the Finnish Ice Service). Another way of ice charting is automatic mapping of the ice concentration field, the principal ice quantity manageable by remote sensing. NSIDC provides global ice charts such as that shown in Figure 2.5 on a daily basis. In Hokkaido, Japan, a coastal radar system was used from 1969 to 2005 for mapping

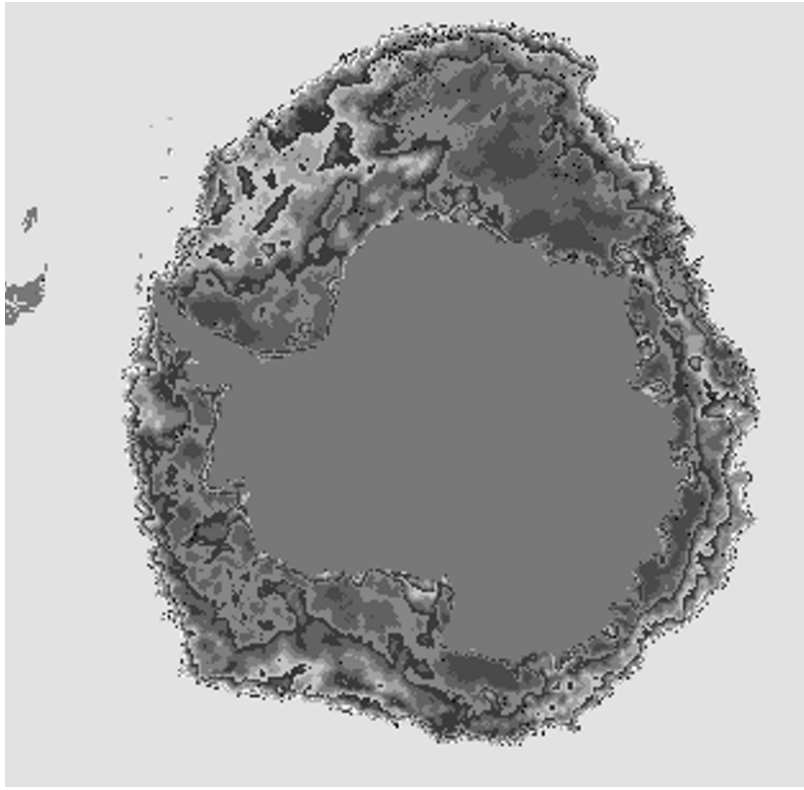

Figure 2.5 Sea ice concentration in the Antarctic based on passive microwave SSM/I data. At the ice edge, compactness increases rapidly to about 80%, while in the inner pack it is mostly 75–90% with a few areas below the 70% level only in the Weddell Sea. NRTSI Product for 2003-10-2 National Snow and Ice Data Center, Boulder, CO.
Reproduced from Cavalieri et al. (1999), with permission from National Snow and Ice Data Center, Boulder, CO.

offshore ice conditions in the Sea of Okhotsk to a distance of 60 km from the coast (`http://www.hokudai.ac.jp/lowtemp/sirl/sirl-e.html`).

The main problem in sea ice charting is how to obtain good ice thickness information – this is also the main problem for the progress of sea ice dynamics theory and modelling.

2.2 ICE FLOES TO DRIFT ICE PARTICLES

2.2.1 Scales

Sea ice mechanics is examined over a wide range of scales. *Microscale* includes individual grains and ice impurities, extending from sub-millimetres to 0.1 m. In the *local scale*, 0.1–10 m, sea ice is a solid sheet, a polycrystalline continuum with a

substructure classified according to the formation mechanism as congelation ice, snow-ice, and frazil ice (Eicken and Lange, 1989). *Ice floe scale* extends from 10 m to 10 km and includes individual floes and ice forms such as rubble, pressure ridges, and fast ice. When the scale exceeds the floe size, the sea ice medium is called drift ice or pack ice and, as in dynamical oceanography, the scales 100 km and 1000 km are *mesoscale* and *large scale*, respectively.

The drift of sea ice takes place on the floe scale and larger. The horizontal structure of sea ice cover is well revealed by optical satellite images (Figure 2.7). The elementary particles are *ice floes*, described by their thickness h and characteristic diameter d. The WMO nomenclature (WMO, 1970) restricts ice floes to those ice pieces with $d > 20$ m; smaller ones are termed *ice blocks*. This is convenient because for ice floes the *aspect ratio* h/d is smaller than about 0.1 and floes included in the definition are flat. The floe size ranges from the lower limit to tens of kilometres. In sea ice dynamics research we consider the drift of individual floes or the drift of a system of ice floes, called a *drift ice field*.

Ice density is taken as a constant ($\rho = 910\,\mathrm{kg\,m^{-3}}$). Therefore, armed with thickness information we can calculate the mass of ice, given as the mass per unit area by $m = \rho h$. In reality, the density varies within $\pm 1\%$ around this reference due to variations in the temperature, salinity and gas content of the ice. Ice floes float

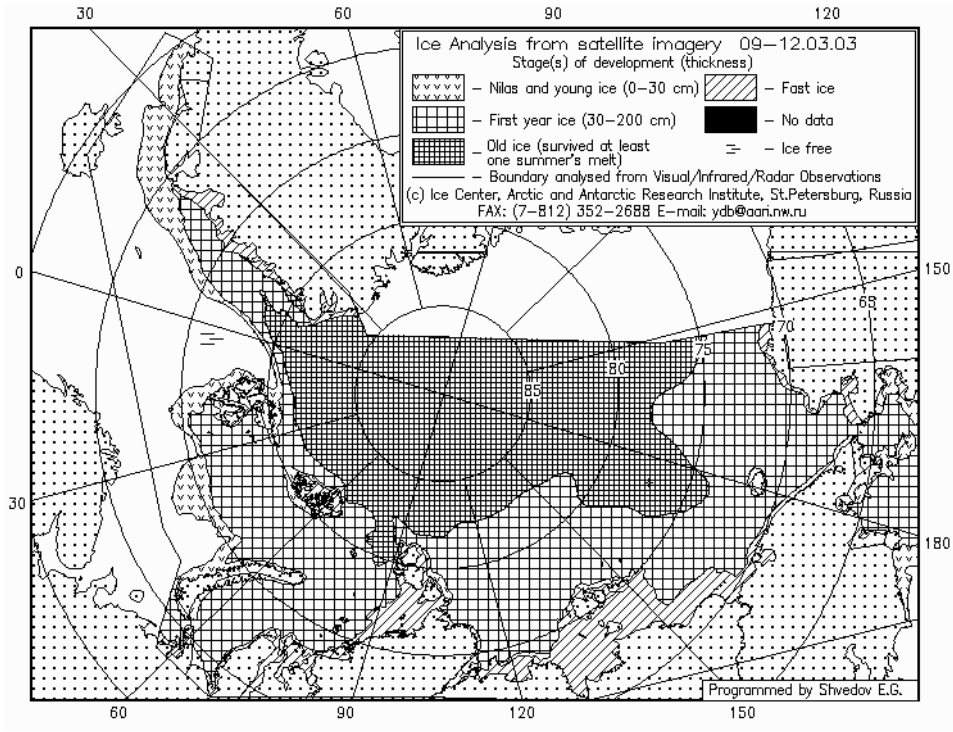

Figure 2.6 Ice chart over the Eurasian side of the Arctic Ocean, 12 March 2003.
Reproduced with permission from Arctic and Antarctic Research Institute, St Petersburg, Russia: htpp://www.aari.nw.ru/

freely, apart from shallow areas where grounding may occur. The portions of an ice floe above and beneath the sea surface are, respectively, *freeboard* (h') and *draft* (h''), $h = h' + h''$. Archimedes' law states that:

$$\frac{h''}{h} = \frac{\rho}{\rho_w} \tag{2.1}$$

where ρ_w is the density of seawater. Since $\rho_w \approx 1028\,\mathrm{kg\,m^{-3}}$ is the density of cold seawater (salinity 35‰, temperature at freezing point), $\rho/\rho_w \approx 0.89$. The potential energy of an ice floe per unit area consists of the freeboard and draft portions, and for floating ice it equals (Rothrock, 1975a):

$$E_p = \rho g \int_0^{h'} z\,dz - (\rho_w - \rho) g \int_{-h''}^{0} z\,dz = \frac{1}{2}\,\frac{\rho(\rho_w - \rho)}{\rho_w}\,g h^2 \tag{2.2}$$

where $g = 9.8\,\mathrm{m\,s^{-2}}$ is acceleration due to Earth's gravity. For ice not floating but supported from the sea bottom, the right-hand equation of Eq. (2.2) is not true.

The behaviour of a drift ice field depends on its horizontal size L and the thickness and size of ice floes. This gives three length ratios: the floe aspect ratio h/d, granularity L/d, and stability h/L. The number of ice floes is proportional to $(L/d)^2$, and the mechanical breakage of an ice sheet mainly depends on h/L and mode of breakage.

Drift ice particles

A drift ice material particle is a set of ice floes. A particle of size D contains $n \approx (D/d)^2$ floes. For the continuum approximation to be valid n must be large: $n > 100$ or equivalently $D/d > 10$. Additionally, the particle size should be much less than the scale of changes or the gradient scale $\Lambda = Q/|\nabla Q|$ where Q is a property of the ice dynamics field. Summarizing, the scales should satisfy:

$$d \ll D \ll \Lambda \qquad \text{for a continuum} \tag{2.3a}$$

or

$$d \sim D \sim \Lambda \qquad \text{for a discrete system} \tag{2.3b}$$

In the real world, the situation is often intermediate (i.e., $d < D < \Lambda$). Depending on the particular question under examination, $d \sim 10^1$–$10^4\,\mathrm{m}$, $D \sim 10^3$–$10^5\,\mathrm{m}$ and $\Lambda \sim 10^4$–$10^6\,\mathrm{m}$. The gradient scale requirement arises for the linear deformation approach to be applicable. Taylor polynomial[2] shows that, e.g., for displacement or velocity, the ratio of the nonlinear residual to the linear term is $\sim \frac{1}{2}|\boldsymbol{x}|/\Lambda$, where $\boldsymbol{x} = (x, y)$ is the horizontal space coordinate vector. Consequently, the condition $D \ll \Lambda$ needs to be satisfied.

[2] Taylor polynomial is written in one dimension as,

$$f(x) = f(0) + \frac{x}{1!}f'(0) + \frac{x^2}{2!}f''(0) + \cdots + \frac{x^n}{n!}f^{(n)}(0) + R_{n+1}(x),$$

where the residual $R_{n+1}(x)$ is of the order of x^{n+1}; for two dimensions $f^{(n)}$ is replaced by $(\partial_x + \partial_y)^n f$ (e.g., Adams, 1995).

In the continuum theory of drift ice, field variables such as ice velocity are defined for each drift ice particle (cf. fluid parcels in fluid dynamics); but, because of the finite size of the floes, their individual features may play a role in the motion of drift ice fields. Thus the theory includes a basic inaccuracy. As D approaches Λ, discontinuities start to build up, and as D approaches d, a system with a single floe or a few floes appears.

Let $h = h(x, y, t)$ stand for the ice thickness in a given point and time; for open water $h = 0$. Define a function "ice", I, by:

$$I(x, y, h_0)\begin{cases} = 0, & \text{if } h(x, y) \leq h_0 \\ = 1, & \text{if } h(x, y) > h_0 \end{cases} \tag{2.4}$$

where h_0 is the *demarcation thickness*. This definition separates thin ice and is convenient in some theoretical considerations. Consider a region Ω in a sea ice pack – it may be a basin, a drift ice particle, or anything between – whose surface area is S. The packing density, or compactness, of ice is defined as:

$$A = \frac{1}{S}\int_{\Omega} I(x, y; 0)d\Omega \tag{2.5}$$

For uniform circular floes, the most open and dense locked packings are $\pi/4 \approx 0.79$ and $\pi/(2\sqrt{3}) \approx 0.91$, respectively (Figure 2.8). The further below 0.79 the packing goes, so contacts between floes become fewer. Since ice floes float nearly on a geopotential surface[3], compactness may easily change. However, at the locked level, further compression necessitates ice breakage and pressure ice formation. The connection between compactness and mean free path l_w is for uniform circular floes

$$\frac{A}{A_{\max}} \approx \frac{d^2}{(d + l_w)^2} \tag{2.6}$$

where $A_{\max}$ is the densest packing for a given set of floes. For $l_w = d$, we have $A/A_{\max} \approx \frac{1}{4}$: and $A/A_{\max} < 0.8$ for $l_w/d > 0.12$, considered to be already in the low stress regime. For distributed floe sizes $A_{\max}$ is in general larger, and $A/A_{\max}$ can be estimated by using averages of d and $d + l_w$ in Eq. (2.6). As the distribution widens, $A_{\max} \to 1$. Thus an important characteristic of an ice floe field is the uniformity of floe sizes.

The *mean ice thickness* $\tilde{h}$ and the *mean ice floe thickness* $\tilde{h}_i$ are defined by:

$$\tilde{h} = \frac{1}{S}\int_{\Omega} h d\Omega = A\tilde{h}_i \tag{2.7}$$

The mean ice floe thickness is thus the mean thickness of the actual ice floe pieces in Ω, while open water is also included in the mean ice thickness. At times, these different thickness definitions have caused confusion. Clearly, we have $0 \leq A \leq 1$ as well as $0 \leq \tilde{h} \leq \tilde{h}_i$. Ice compactness and mean ice floe thickness are the fundamental quantities for the mechanical properties of drift ice. Other ice quantities are integrated over drift ice particles or any regions in similar ways.

[3] Surface normal to the local gravitational acceleration (true horizontal).

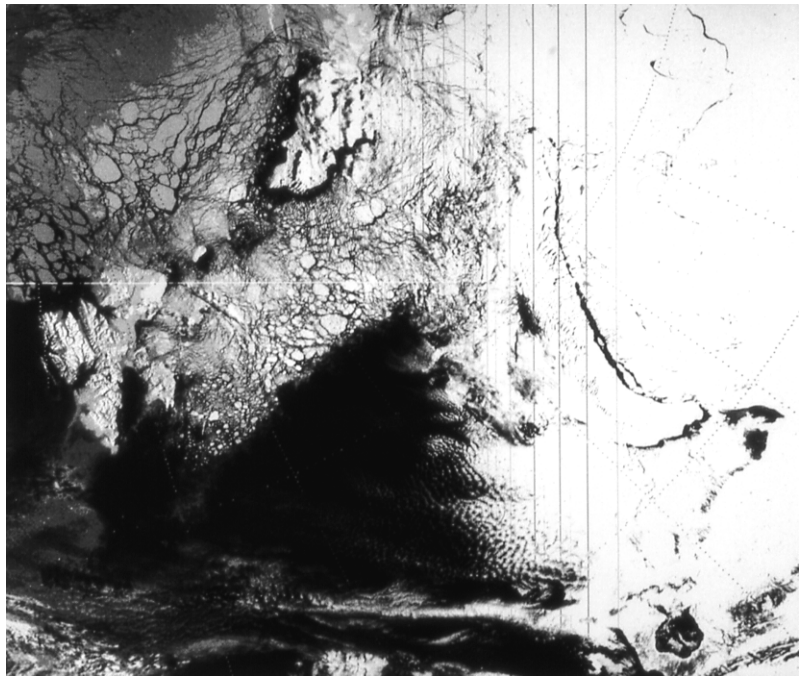

Figure 2.7. An optical channel NOAA–6 image over the Barents Sea and Arctic basin north of it, 6 May 1985. Svalbard is shown on the left, Franz Joseph's land up in the middle, and Novaya Zemlya on the right. The east side is cloudy, but elsewhere drift ice floes can be seen. The image was received at the Tromsø receiving station, Norway.

The granular medium approach was introduced for drift ice in the 1970s, taking ideas from soil mechanics (Coon, 1974), resulting in poly-granular continuum models. More recently, discrete particle models have been used and found to work well in the floe scale (e.g., Løset, 1993; Hopkins, 1994); but for larger scale drift ice problems they have not overcome continuum models. A possible step between discrete and continuum models could be the "particulate medium" approach (Harr, 1977). This is composed of a complex conglomeration of discrete particles, in arrays of varying shapes, sizes and orientations. The laws of mechanics are derived from probabilistic viewpoint.

2.2.2 Size and shape of ice floes

Floe size distribution

Sea ice floes break continuously into smaller pieces, and in the cold season they are at the same time frozen together into larger pieces. Floe size distributions show statistical regularity based on random floe break-up mechanisms. A characteristic floe diameter d can be defined from its surface area S_f as $d = \sqrt{4S_f/\pi}$. For a circle, d

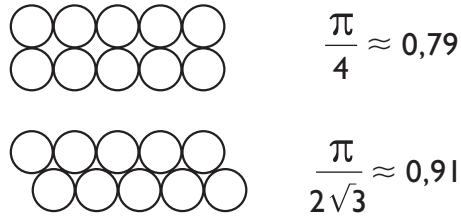

Figure 2.8 Open and dense locked packings of uniform circular ice floes.

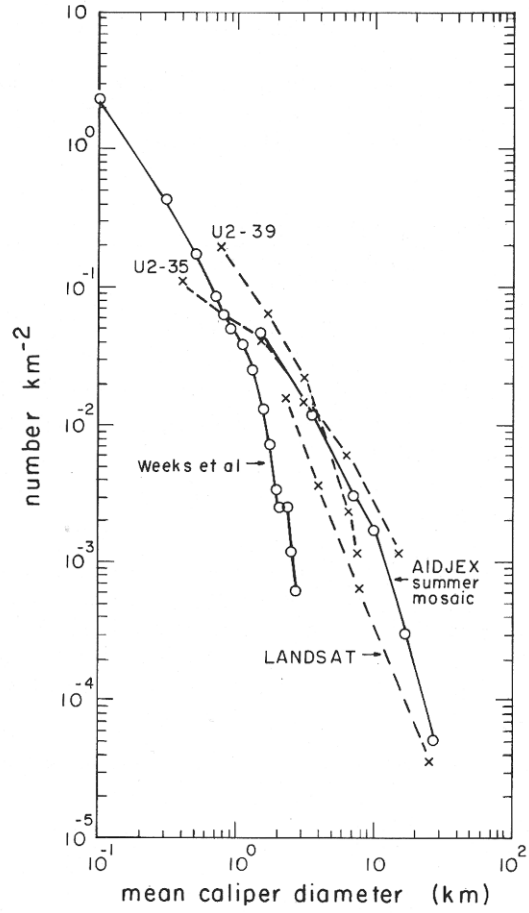

Figure 2.9 Floe size distributions from the Arctic Ocean.
Reproduced from Rothrock and Thorndike (1984), with permission from the American Geophysical Union.

equals the diameter. Rothrock and Thorndike (1984) introduced their mean "caliper diameter", equal to the directional average of the opening the floe goes through. It is approximately equal to the π^{-1} times the perimeter. For a circle, this is therefore equal to the diameter. Actual floe size observations cover a certain range $d_0 \leq d \leq d_1$, where d_0 and d_1 are the minimum and maximum resolution, respectively. Floes are usually examined from satellite images, aerial photographs or ship-borne oblique-angle video records.

The distribution of floe sizes is usually presented using the spatial density $p(d)$ (i.e., number of floes in different size classes). A more preferable way is, however, to consider the areal coverage. The area of the floes larger than size d is:

$$Q(d) = \int_d^\infty r^2 p(r)\, dr \tag{2.8}$$

Then q-fractiles $d^{(q)}$ can be defined through $Q(d^{(q)}) = qQ(0)$ (i.e., floes larger than $d^{(q)}$ cover the fraction of q of the total ice area). A natural representative floe size is $d^{(0.5)}$, the median. In soil mechanics (e.g., Harr, 1977), $d^{(0.1)}$ defines the effective size and the ratio $d^{(0.6)}/d^{(0.1)}$, is known as the uniformity coefficient.

Observed floe size distributions show regular features. The spatial density function steadily falls toward larger values with no local peaks or gaps at least within the observation windows (Figure 2.9), and the shape of the distribution may be derived from rather simple fracturing principles (Figure 2.10). Eq. (2.8) tells us that if the spatial density falls as d^{-2}, the distribution of the areal coverage of ice floes is uniform.

Fractal geometry models lead to *power law* size distributions (e.g., Korvin, 1992). The probability density is:

$$p(d; n) \propto d^n \tag{2.9}$$

In a d-band where n = constant, *self-similarity* holds. Within a self-similar band the geometric structure is independent of the scale, reflected by photographs showing similar floe systems in different scales within the self-similar band, and a measure stick needs to be added for the scale information (Figure 2.11). Such scale invariance is quite common in geophysical data. For all power laws we have $\int_0^\infty x^n dx = \infty$. Floes are smaller than the basin and therefore the integral should be taken from 0 to basin size (L) only. Then the integral is finite for $n > -1$; however, this is not necessary since for a fractal system the number of ice floes is infinite. The necessary condition is that the area of ice floes is finite:

$$\int_0^L x^{n+2} dx < \infty \tag{2.10}$$

which means that $n > -3$. Observations usually suggest that $-3 < n < -1$ for $d > 20$ m (i.e., for ice pieces defined as floes in the WMO, 1970 nomenclature).

Example Take $n = -2$. Then

$$\frac{Q(d)}{Q(0)} = 1 - \frac{d}{d_1}$$

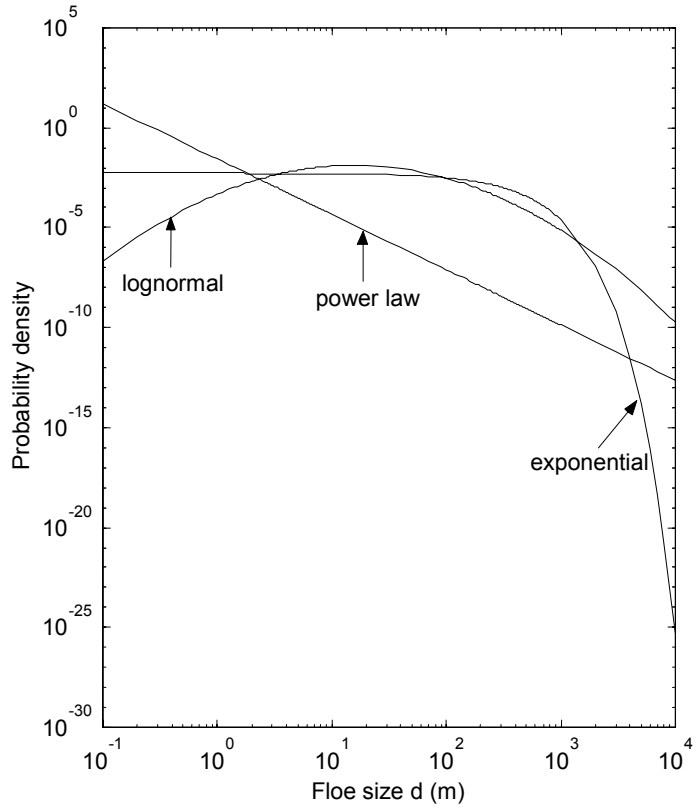

Figure 2.10 The forms of the power law, exponential, and lognormal distributions for the floe size, scaled with median equal to 500 m.

where d_1 is the maximum floe size. The distribution of floe size in terms of areal coverage is uniform from zero to d_1, as sometimes observed (e.g., Leppäranta, 1981b). The median floe size is $d_1/2$, and any q-fractile is given by $d_q = d_1(1-q)$. The uniformity coefficient is $4/9 \approx 0.44$. For $n < -2$ small floes are areally dominant while for $n > -2$ the opposite is true. The exponent obtained from observations therefore illustrates how fractured the ice field is.

In the data of Rothrock and Thorndike (1984) the mean caliper diameter followed the power law ($d > 100$ m) with $-2.5 < n \leq -1.7$. For the spring season in the Baltic Sea, Leppäranta (1981b) obtained $-3 < n < -2$, decreasing in the course of the spring melting season. This illustrates that the area of small floes increases at the cost of large ones. Cases with $n \leq -3$ have been occasionally reported; then the ice floe field must be understood as a multi-fractal where $n \leq -3$ holds in the observation window but as $d \to 0$ the power must go above -3.

A classical *random breakage* model, where the breakage probability is independent of the floe size, gives the *logarithmic normal distribution* (Kolmogorov, 1941).

Then, by definition, $\log d$ is normally distributed, say, with mean M and variance s^2. Define a characteristic floe size d_* by $\log d_* = M$. The probability density then reads:

$$p(d; d_*, s^2) = \frac{1}{ds\sqrt{2\pi}} \exp\left[\frac{-\log(d/d_*)}{2s^2}\right], \quad d > 0 \tag{2.11}$$

The median is then equal to d_*, the mode and mean are $d_* \exp(-s^2/2)$ and $d_* \exp(s^2/2)$, respectively, and the variance is $d_*^2 \exp(s^2)[\exp(s^2) - 1]$ (e.g., Crow and Shimizu, 1988). The parameter s^2 is regarded as the shape parameter of the distribution. It is dimensionless since by definition s^2 is the average of $(\log d - \log d_*)^2 = \log(d/d_*)^2$. The median of the distribution Q for floe coverage becomes $d_* \exp(2s^2)$. The distribution has a positive mode, which is not far from zero and usually not covered in observational data; thus the existence of such a mode in nature is not clear.

Logarithmic normal distribution has been found to fit observations as well as the power law. The reason is likely due to that these two distributions differ remarkably only at very small floe sizes (see Figure 2.10), normally not covered by the observation window.

If the breakage probability is proportional to the floe size, the spatial Poisson process results, leading to the *exponential distribution* of floe size:

$$p(d; \lambda) = \lambda \exp(-\lambda d) \tag{2.12}$$

where λ is the distribution shape parameter. This is analogous to the distribution of waiting times of customers in the theory of temporal Poisson processes. Density can be directly integrated: the relative areal coverage of floes larger than d is $Q(d) = [1 + \lambda d + \frac{1}{2}(\lambda d)^2] \exp(-\lambda d)$. The median of the distribution Q can be numerically solved as $d_{0.5} \approx 2.67\lambda^{-1}$. Exponential distribution is quite different from the other two and is not much supported by observations.

According to the present knowledge, only in the case of small floes can physical mechanisms be found to produce a favourable floe size. An important property of floating ice is its *characteristic length*:

$$l_c = \sqrt{\frac{Yh^3}{12\rho_w g(1 - \nu^2)}} \tag{2.13}$$

where Y is Young's modulus and ν is Poisson's ratio; representative values for them are $Y \approx 3$ GPa and $\nu = 0.3$ (e.g., Mellor, 1986). For $h = 1$ m, we have $l_c = 12.7$ m. The length of flexural waves of an elastic ice beam on water foundation under a point load equals $2\pi l_c$. When ice floes break under rafting the size of pieces is $\frac{1}{4}\pi l_c$ (Coon, 1974).

An eye-striking ice field is *pancake ice* (see Figure 2.3), which is often found in the marginal ice zone when the ice cover is extending in turbulent oceanic surface layer conditions. Frazil crystals join in the surface to plate aggregates, which collide with each other and become rounded. Due to its visual appearance, this ice type is called pancake ice, and the size of the "pancakes" is up to a few metres. They grow by mechanical scavenging and rafting up to thickness of consolidation, which has been reported to be around 60 cm in Antarctic seas (Doble, 2008).

At the ice edge, reflection and penetration of swell takes place (Wadhams, 1978; Squire *et al.*, 1998; Squire, 1998). A penetrating swell becomes damped with distance from the ice edge. The wave energy as a function of distance (x) from the ice edge is:

$$E(x) = E(0)\exp(-x/l_s), \tag{2.14}$$

where l_s is the attenuation distance. Long waves penetrate more easily. In heavy, compact ice, $l_s \approx 1\,\text{km}$ for short waves (100 m) and 5 km for long swells. The dominant wavelength increases exponentially from the ice edge and waves easily break floes down to one-half wavelengths. Consequently, the floe size should increase exponentially from the ice edge, as long as there is enough energy in the wave field for floe breakage. This is observed in the MIZ in a qualitative sense: floes are small, $\sim 10^2$ m and there is general increase in floe size with distance from the ice edge. But no actual e-folding length scales for the floe size have been recorded, the signal being contaminated by strong mixing and the thermo-mechanical decay of ice floes.

Random breakage seems to explain the floe size distributions well, with the breakage probability independent of the floe size, apart from the breaking by waves. Small floes may have preference sizes but their size distributions have not been studied to any great extent. The question is then how to formulate the random breakage probability that would lead to the exact form of the distribution (Lensu, 2003). Ice floes have more or less randomly distributed defects; that is, cracks due to thermal, hydrostatic (from non-uniform ice thickness), tidal, and wind loads.

Shape of ice floes

Sea ice floes are convex. Wintertime ice floes are typically rectangular or pentagonal, while in summer the sharp corners erode and the floes become rounded (Timokhov, 1998).

The shape of a floe can be quantified using its major axis ($d_{\max}$), minor axis ($d_{\min}$), and characteristic diameter (d_*), where $d_{\min}$ is the minor axis corresponding to the smallest opening through which the floe may penetrate, $d_{\max}$ is the length perpendicular to the direction of the minor axis, and d_* is the diameter of the circle with the same surface area as the floe. The shape parameters are:

$$\upsilon = \frac{d_{\max}}{d_{\min}}, \quad \kappa = \frac{d_*^2}{d_{\max} d_{\min}} \tag{2.15}$$

where υ is elongation and κ is shape factor. The latter equals unity for elliptical ice floes and $\pi/4$ for rectangular floes. In a study in the Baltic Sea (Leppäranta, 1981b), elongation was mostly 1–2 and the shape factor was 0.7–1.0. There are not enough floe shape results available to state how typical these Baltic Sea properties are.

Floe information in drift ice mechanics

Granular media consist of grains and voids (e.g., Oda and Iwashita, 1999). Their macroscopic behaviour is determined by the grains, their arrangements, and

interacting forces between the grains. Some efforts have been made for granular medium approach in sea ice dynamics with floes as individual grains, but in essence all mesoscale and large-scale sea ice models are based on the continuum theory. Linkages between floe scale mechanics and continuum mechanics are not clear.

Ice floe information is implicitly included in the continuum theory in that the validity of continuum hypothesis requires that the drift ice particle size should be an order of magnitude greater than the characteristic floe size (see Eq. 2.3). Otherwise, it is not yet clear how useful the floe size and shape information really are in the continuum of sea ice dynamics. The granular medium approach would be the way to link floe scale mechanics and continuum mechanics together as well as to understand properly the physical meaning of continuum model parameters. In local-scale granular models, both floe size and shape influence the results (and in particular, the friction coefficient between ice floes is important).

When ice floes reach their maximum packing density, the nature of material behaviour changes. When compactness is low, floe interactions do not transmit forces well and the level of stress is very small. When the ice pack closes up and the stress increases to a significant level, floes make contact with others, group together, and then lose many of their individual features. Nevertheless, the stress field still depends on the shape of ice floes throughout the total area of contact surfaces. This may be a reason for stress fields being lower in summer conditions. Drag forces between air and ice, and between water and ice depend on the size and shape of ice floes (Zubov, 1945; Andreas *et al.*, 1984). When floes are smaller their number is larger and consequently there are more floe edges to provide form drag. This feature, however, disappears when the floes close up.

Ovsienko (1976) was the first work to include floe size in a drift ice model, but without mechanical interaction. Shen *et al.* (1986) developed a theory based on momentum transfer by floe collisions using uniform and circular ice floes. For such floes a discrete particle model with full floe–floe interaction was studied by Løset (1993). Hopkins and Hibler (1991) and Hopkins (1994) examined the sea ice-ridging process with a discrete particle model and the floes could be of general polygonal shape.

The poor understanding of the role of horizontal floe characteristics is largely due to the fact that in sea ice dynamics the thickness of ice floes is the principal floe property, their horizontal size being given less prominence. However, the size and shape of ice floes show much more regularity than the thickness field, and they can be easily monitored by remote sensing methods. Consequently, floes would be quite useful in sea ice dynamics modelling by adding their evolution laws for examinations by model simulations against observations. The floes would serve as test material and tracers for model ice mechanics.

In applied fields, floe size can be an important property to predict. Loads on structures caused by individual drifting floes depend on the floe size, and drift and dispersion of oil spills in an ice-covered sea are sensitive to ice compactness and floe geometry. Therefore, although the floe size and shape would not exert much influence on the dynamics of ice itself, they can be necessary to be kept in the model as a field, which changes by advection, diffusion, mechanical breakage, and thermodynamics. In short-term forecasting, just advection and diffusion would be a useful approach.

2.3 SEA ICE GROWTH AND MELTING

2.3.1 Freezing of seawater

The freezing point (T_f) of normal seawater is $-1.9°C$, while the temperature of maximum density (T_D) is well below that[4]. Therefore the density of seawater increases throughout the cooling process and vertical convection penetrates to the halocline or, if halocline does not exist, to the sea bottom. Brackish waters behave as fresh water lakes in that $T_f < T_D$. The onset of freezing depends on the external conditions (Weeks and Ackley, 1986; Eicken and Lange, 1989; Weeks, 1998a). In case of weak wind a thin primary ice layer forms first, and then *congelation* ice crystals grow down from the bottom of the primary ice. In windy conditions *frazil ice* crystals are first formed, moving free in the turbulent surface layer and joining into a solid sheet when the buoyancy overcomes the turbulence. This is also the initial stage in pancake ice formation. In shallow and well-mixed waters frazil may also attach into the sea bottom to form *anchor ice*. Snow falls on the top of ice and may form slush to further freeze into *snow-ice*. In Antarctic shelf waters, so-called *platelet ice* forms as glacial melt water rises from bottom of ice shelves, becomes supercooled, and crystallizes onto sea ice bottom as large platelets. Thus a sea ice sheet in general consists of layers of different forms of ice. Good references for sea ice thermodynamics are Maykut and Untersteiner (1971), Makshtas (1984) and Shirasawa *et al.* (2005).

Congelation ice crystals grow down from the ice–water interface, and the crystals are columnar, diameter 0.5–5 cm and height 5–50 cm. The growth is limited by the insulation effect of the ice, and the thicker the ice, the lower the growth rate will be. In the Arctic Ocean, congelation ice is the dominant ice type. Frazil ice forms in open water areas. The crystals are small (1 mm or less). The growth rate can be fast because of intensive heat losses from open water to cold atmosphere and the growth is not strongly limited as long as there is open water present. In Antarctic seas, frazil ice is the dominant ice type. There it is also typical that frazil crystals join in the surface to form pancake ice.

Snow-ice forms on top of the ice from slush, generated by snow and liquid water available from flooding, liquid precipitation or melt water of snow. The crystals are small as in frazil ice. Growth of snow-ice is limited by the presence of snow and availability of liquid water. The most common formation mechanism is flooding, which becomes possible when the snow weight has forced the ice sheet below the water surface level, that is:

$$\frac{h_s}{h} > \frac{\rho_w - \rho}{\rho_s} \tag{2.16}$$

where h_s is snow thickness and ρ_s is snow density. Since $(\rho_w - \rho)/\rho_s \approx 1/3$, the thickness of snow needs to be at least one-third of the thickness of ice for the flooding to occur. Since growth limitation is provided by the ratio h_s/h, snow-ice formation is

[4] $T_f[°C] = -57.5S + 54.0915S^{3/2} - 215.4996S^2 - 7.53 \times 10^{-3}p$ [bar], where S is salinity and p is pressure (UNESCO, 1981).

common in Antarctic first-year ice and in low latitude seas, such as the Baltic Sea and the Sea of Okhotsk, where snow accumulation is large and ice is not too thick.

By thermal processes first-year polar sea ice grows to 1–2 m thickness and multi-year ice to 3–4 m. In the seasonal sea ice zone the thickness is mostly less than 1 m. Thermally grown ice is also called *undeformed ice*, as distinct from *deformed ice* forming in mechanical deformation processes. Sea ice thermodynamics forms a coupled temperature–salinity problem (e.g., Maykut and Untersteiner, 1971), but in thermodynamic models so far salinity has been a prescribed function of time and depth. In sea ice growth heat flow is strongly vertical and transfer of heat through ice is slow. The heat diffusion coefficient is $\approx 1 \times 10^{-6}\,\mathrm{m^2\,s^{-1}}$, which gives the length scale of 4 m in a half year's time. Thus in floe scale or larger scale processes ice growth can be taken as a local vertical process. Melting of sea ice can, on the other hand, take place also laterally, when heat absorbed by leads is transferred to lateral boundaries of ice floes (see Rothrock, 1986).

The sea ice nomenclature (WMO, 1970) connects thicknesses to types of undeformed ice as discussed in Section 2.1. New ice forms grow up to 10 cm, young ice is 10–30 cm, and first year ice is divided into thin (30–70 cm), medium (70–120 cm), and thick (greater than 120 cm) categories. Undeformed first-year ice can be as much as 2 m thick, while the equilibrium thickness of undeformed multi-year ice is 3–4 m (Maykut and Untersteiner, 1971). The terminology is based on ice conditions in the Arctic seas; it is not fully used in subpolar regions because of inconsistencies in the use of common language: for example, in the Baltic Sea, the thickest ice could be "thin first-year ice", and "young ice" could be several months old and as old as any ice there. It is therefore preferable to give the numerical value of thickness.

The impurities of sea ice consist of *brine*, *solid salt crystals*, *gas bubbles* and *sediments*. The first two types result from growing sea ice capturing salts (Weeks, 1998a). They constitute the most important impurities to the physical properties of sea ice; in particular, the mechanical strength of sea ice sheet depends primarily on the brine volume. The volume fraction of gas bubbles is $\nu_a \sim 1\%$, and the bubble size is in the range 0.1–10 mm. Sediment particles originate from the water body, harvested by frazil ice, from sea bottom when anchor ice rises up due to its buoyancy, and from atmospheric fallout accumulating on the ice during the ice season. Sediments may influence the properties of ice and they may also have a significant role in transporting matter, especially pollutants.

2.3.2 Ice growth

Thermodynamic growth of congelation ice is a classical geophysical problem, where approximate analytical solutions are available (Figure 2.12). Weyprecht (1879) showed, based on his data from the Arctic, that sea ice thickness is proportional to the square root of the sum of freezing-degree-days, which is defined as:

$$S_0(t) = -\int_0^t [T_0(t') - T_f]dt' \tag{2.17}$$

(a)

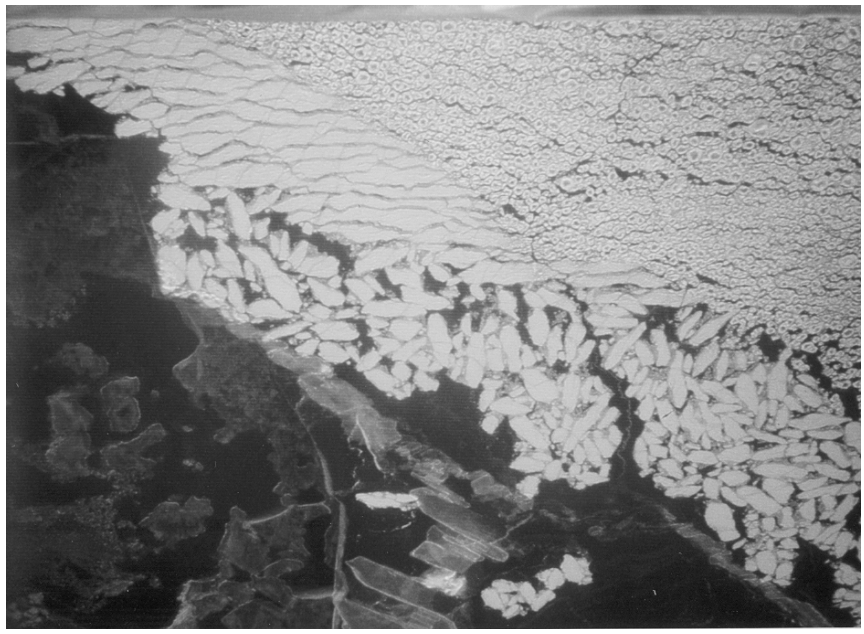

(b)

Figure 2.11 Sea ice floes shown in pictures over different scales. (a) Thin ice floes and rafted ice, altitude 500 m. (b) Oblique angle over ridged ice, altitude 1 km.

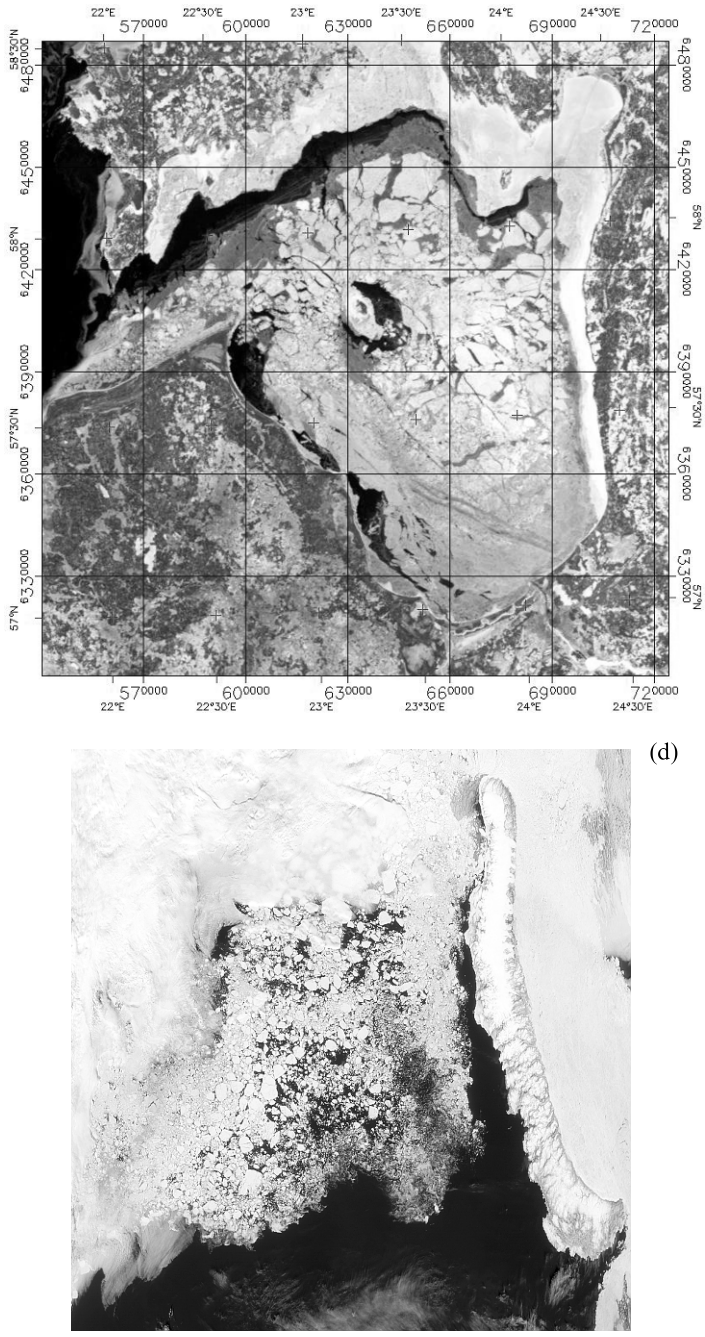

Figure 2.11 (continued). (c) Gulf of Riga, basin size 120 km. (MODIS image of NASA's Terra satellite.) (d) Barents Sea – the length of Novaya Zemlya on the right is about 1000 km (© NASA, Visible Earth Team).

where T_0 is the surface temperature (assuming that $T_0 \leq T_f$). The physics of this result was then explained by Stefan (1891). The thermodynamics of congelation ice follows the Fourier heat conducting law:

$$\frac{\partial}{\partial t}(\rho c T) = \frac{\partial}{\partial z}\left(\kappa \frac{\partial T}{\partial z}\right) + q \tag{2.18}$$

where c is specific heat, κ is thermal conductivity, and q is the absorption of solar radiation within the ice sheet, $q = q(z)$.

Ignoring thermal inertia, solar radiation and heat flux from water to the ice bottom, and assuming constant thermal conductivity, a linear temperature profile results. The slope of this profile gives the conduction of heat, which must correspond to the latent heat release due to congelation ice growth at the bottom of the ice sheet:

$$\rho L \frac{dh}{dt} = \kappa \left.\frac{\partial T}{\partial z}\right|_{z=h^n} = \kappa \frac{T_f - T_0}{h} \tag{2.19}$$

This is the Stefan's model (Stefan, 1891). The thicker the ice, the slower is the conduction, and hence the rate of ice growth decreases when the ice becomes thicker. With initial value $h(0) = 0$, Eq. (2.19) can be directly integrated into $h = a\sqrt{S_0}$, where $a = \sqrt{2\kappa/(\rho L)} \approx 3.3\,\mathrm{cm\,d^{-1/2}\,{}^\circ C^{-1/2}}$ is the growth coefficient. It is also seen that growth of very thin ice rarely would exceed $10\,\mathrm{cm\,d^{-1}}$ and for 1 m thick ice the growth rate is already below $1\,\mathrm{cm\,d^{-1}}$.

A major problem with the Stefan's model is that the surface temperature is required. This is not usually known and therefore the freezing-degree-days S based on air temperature rather than surface temperature is used; i.e., in the integral in Eq. (2.17) $T_0 - T_f$ is replaced by $T_a - T_f$, where T_a is air temperature. Zubov (1945) added air–ice heat exchange to the model, and based on the continuity of heat flow resulted in the pair of equations:

$$\rho L \frac{dh}{dt} = \kappa \frac{T_f - T_0}{h} = K_a(T_0 - T_a), \quad T_0 \geq T_a \tag{2.20a}$$

where K_a is ice–air heat transfer coefficient. Note that we must have here $T_0 \geq T_a$ for the ice to grow (i.e., days $T_0 < T_a$ are ignored). The solution is:

$$h = \sqrt{a^2 S + \delta^2} - \delta \tag{2.20b}$$

where $\delta = \kappa/K_a \approx 10\,\mathrm{cm}$ is the insulation efficiency of the atmospheric surface layer. The classical Stefan's law is recovered by letting $\delta \to 0$, which means physically that the atmosphere can take any heat, which is coming through the ice.

Example 100 days with the air temperature of $-10^\circ\mathrm{C}$ gives $S = 810^\circ\mathrm{C \cdot day}$, and then Zubov's model gives $h = 94.4\,\mathrm{cm}$ and Stefan's model gives 84.9 cm. The square root law describes well how the ice insulates itself from the cold atmosphere during the growth process. Especially when the ice is thin, Stefan's model strongly overestimates the ice growth. For $S = 20^\circ\mathrm{C \cdot day}$, the Zubov and Stefan models give 7.9 cm and

14.8 cm, respectively. Inversely, we can see that since first-year ice thickness is 2 m at highest in the Arctic Ocean, the freezing-degree-days must sum there to 4000°C · day.

The main problem in Zubov's model is the lack of snow. Heat flux through snow is $\kappa_s \Delta T/h_s$, where κ_s is thermal conductivity of snow and ΔT is the temperature difference across the snow layer. This can be added as a new equation into the Zubov's model (Eq. 2.20a), but in general, analytic solutions are no longer possible since the thickness and conductivity of snow depend on time. For illustration, if they are constant, the solution is similar to Zubov's case, but the insulation layer thickness δ is replaced by:

$$\delta^* = \left(1 + \frac{K_a h_s}{\kappa_s}\right)\delta \tag{2.21}$$

Since $\kappa_s/K_a \sim 2$ cm, just a 2-cm snow layer will double the insulation effect of the atmospheric surface layer. The insulation effect of the snow is limited by the buoyancy of ice, since snow accumulation may lead to flooding and further to snow-ice formation (see Eq. 2.16). If snow thickness increases with ice thickness but not enough for slush formation, the maximum insulation effect reduces the ice thickness to half as compared with the growth of snow-free ice (Leppäranta, 1993).

Snow-ice grows from slush on top of the ice. Latent heat released in freezing needs to be conducted through the dry snow above slush only. Also, less latent heat needs to be released than in the growth of congelation ice since the slush already contains ice crystals. The growth equation reads:

$$\rho\nu L \frac{dh_{si}}{dt} = \kappa \frac{T_f - T_s}{h_{si}} = \kappa_s \frac{T_s - T_0}{h_s'} = K_a(T_0 - T_a), \quad T_0 > T_a \tag{2.22}$$

where $\nu \sim 50\%$ is the water content of the slush layer, h_{si} is snow-ice thickness, T_s is temperature at the snow-ice-snow interface and h_s' is the thickness of dry snow above snow-ice–slush layer. This is as Zubov's model except that the latent heat of freezing is reduced by the factor of ν. The fractions of congelation ice and snow-ice depend on snow accumulation history (Figure 2.13). Assume that in an extreme situation, when the slush is produced by flooding, the rate of snowfall is just enough to produce continuous growth of snow-ice and no congelation ice forms. Then the ice thickness becomes 70% of the snow-free congelation ice case (Leppäranta, 1993).

In spring, the day-and-night melting–freezing cycle gives additional growth to the snow-ice layer. Shirasawa *et al.* (2005) reported on average 24 cm snow-ice growth in the melt–freeze cycles in April offshore Sakhalin in the Sea of Okhotsk. Close to the edge of the seasonal sea ice zone liquid precipitation may significantly contribute into the accumulation of the snow-ice layer. For snow-ice formation by melt–freeze cycles or liquid precipitation, the limiting factor is the snow. In the former case the snow-ice layer may grow at most to $(\rho_s/\rho)h_s$, while in the latter case the limit is h_s. When there is no snow left, any water on ice may freeze into surface ice. Together, snow-ice and surface ice are called *superimposed ice*, a term familiar from glaciology.

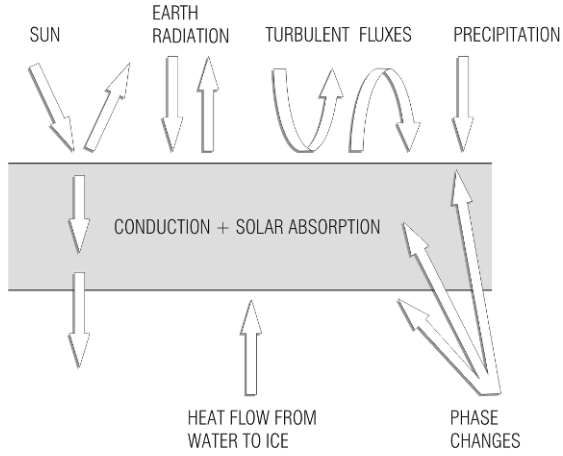

Figure 2.12 Schematic illustration of sea ice thermodynamics. Ice grows and melts at the boundaries and in the interior, forced by heat exchange with air and water and by radiation.

Frazil ice growth is a dynamic-thermodynamic phenomenon. Frazil ice crystals are generated in turbulent open water spots, and they are then transported further by ocean surface layer currents. The rate of production of frazil crystals, h_F is:

$$\frac{dh_{\mathrm{F}}}{dt} = -\frac{Q_n}{\rho L} \tag{2.23}$$

where Q_n (here $Q_n < 0$) is the net heat gain by the ocean surface layer (the full heat budget with net gain will be discussed in Section 2.3.5). Note that the dimension of h_F is length and this quantity can be interpreted as the production of volume over unit surface area. What simplifies the problem is that we can assume $T_0 = T_f$. With low air temperature and moderate or stronger wind, the sensible heat flux is dominating.

Example. If $T_a = -10^{\circ}\mathrm{C}$ and $U_a = 10\,\mathrm{m\,s^{-1}}$, we have $Q_n \sim 200\,\mathrm{W\,m^{-2}}$, which means frazil ice production of $\sim$6 cm day^{-1}. The corresponding growth using Zubov's model would be 3.8 cm starting from zero and 2.1 cm starting from 10 cm.

Frazil ice crystals flow in the turbulent boundary layer. They may attach to the bottom of the ice sheet downstream, attach to the sea bottom in shallow areas, or form an ice layer in the opening where they have formed after the buoyancy of ice crystals has overcome the turbulence. Frazil ice layers can be recognized in the ice sheet later on[5]. From sea ice dynamics point of view, frazil ice formation means rapid production of ice and increase of ice mass as well as, in many situations, rapid closing of open water areas. However, if frazil is transported away, open water becomes semi-persistent and continues long time with its high rate of ice production,

[5] Frazil ice and snow-ice crystals are similar in the crystal structure but can be distinguished using oxygen isotope ratios since snow-ice contains fresh precipitation.

as is the case in many polynyas. In turbulent conditions with surface waves, frazil ice formation is the first stage in the development of pancake ice, a common process in Antarctic sea areas (Doble, 2008).

2.3.3 Melting of sea ice

Sea ice melts from the top surface by atmospheric and solar heat fluxes, in the interior by solar radiation, and from the bottom surface by oceanic heat flux. Boundary melting follows simply from a positive heat balance:

$$\frac{dh_0}{dt} = -\frac{Q_n}{\rho L}, \quad \frac{dh_b}{dt} = -\frac{Q_w}{\rho L} \tag{2.24}$$

where Q_w is the oceanic heat flux. Incoming solar radiation, Q_s, is divided into three parts by the sea ice medium: absorption at the surface, penetration through the surface, and reflection and scattering back to atmosphere (see Perovich, 1998). The "surface" is here a very thin top layer where infrared radiation is absorbed. The penetrating part is light: $Q_{s+} = (1 - \alpha)\gamma Q_s$, where α is albedo and γ is the fraction of the optical band in solar radiation. Since the optical thickness of sea ice is 0.5–5 m, depending on the quality of ice, part of sunlight goes through ice into the water. For the light transfer through the ice, the exponential attenuation law is normally employed:

$$\frac{\partial Q_{s+}}{\partial z} = -\lambda Q_{s+} \tag{2.25}$$

where λ is the attenuation coefficient, $\lambda \sim 1\,\mathrm{m}^{-1}$ for congelation ice and $\lambda \sim 10\,\mathrm{m}^{-1}$ for snow-ice (Perovich, 1998). Radiation absorbed inside the ice is used for internal melting. Field data have shown that in lake ice the boundary melting and internal melting are of the same magnitude (Jakkila *et al.*, 2009), and it can be anticipated that for sea ice the internal melting would be as important. What makes the treatment of solar radiation difficult for sea ice thermodynamics is the large space–time variability of optical properties of sea ice during the melting season.

Oceanic heat flux comes from the oceanic boundary layer beneath the ice and can be estimated using the turbulent boundary layer theory (see McPhee, 2008). The bulk formula is written

$$Q_w = \rho_w c_w C_{wH}(T_w - T_f)|\boldsymbol{U}_w - \boldsymbol{u}| \tag{2.26a}$$

where c_w is specific heat of seawater, C_{wH} is ice–water heat exchange coefficient, and T_w and $\boldsymbol{U}_w$ are water temperature and water velocity, respectively. In contrast to atmospheric heating, oceanic heat flux is always positive toward ice and thus it melts ice though the whole year, i.e., heat flows only from water to ice. At the bottom of sea ice we have the boundary condition:

$$\rho L \frac{dh}{dt} + Q_w = \kappa \left.\frac{\partial T}{\partial z}\right|_{z=h^n} \tag{2.26b}$$

In the melting season the right-hand side is zero, and oceanic heat flux is all used for melting of ice.

Much research work has been done on the heat fluxes at the upper surface. But the lower boundary is much less known, due to greater observational difficulties and also due to the uniqueness of the ice–ocean interaction. There was a large interdisciplinary study of the Surface Heat Budget of the Arctic Ocean (SHEBA), consisting of a year-long field experiment from October 1997 through October 1998 in the Chukchi Sea (e.g., Perovich *et al.*, 2003). The oceanic heat flux during the SHEBA summer ranged from 10 to $40\,\mathrm{W\,m^{-2}}$, and the average bottom melt rate during the summer was $0.50\,\mathrm{cm\,d^{-1}}$, equivalent to an average oceanic heat flux of $17.5\,\mathrm{W\,m^{-2}}$ (Perovich *et al.*, 2003). Undeformed landfast ice cover, such as in a lake, lagoon, fjord, bay or in a sheltered coastal region, works as a stable platform for ocean boundary layer investigations, and also there the ice grows mainly by thermodynamics. According to measurements over landfast ice the oceanic heat flux has been found in the range of 1–$100\,\mathrm{W\,m^{-2}}$, which makes a significant contribution to the ice thickness evolution (e.g., Shirasawa *et al.*, 2006). Uusikivi *et al.* (2006) observed very small heat fluxes of $1\,\mathrm{W\,m^{-2}}$ or less in a laminar flow and/or laminar-turbulent transition regime under sheltered coastal landfast ice covers in the Baltic Sea.

The oceanic heat flux Q_w can be included in Zubov's model by adding it to the left term in Eq. (2.20a). The growth equation reads then:

$$\rho L \frac{dh}{dt} + Q_w = \frac{a^2}{2} \cdot \frac{T_f - T_a}{h + d} \quad (T_f > T_a) \tag{2.27}$$

A general analytical solution is no more possible. If $T_a = \text{constant}$, it is seen that there exists an equilibrium solution with $dh/dt = 0$:

$$h_q = \frac{a^2}{2} \cdot \frac{T_f - T_a}{Q_w/\rho L} - d \quad (T_f > T_a) \tag{2.28}$$

If the oceanic heat flux is strong, it may become a limiting factor in ice growth by ice thickness reaching the equilibrium. For example, if $T_f - T_a = -15^\circ\mathrm{C}$ and $Q_w = 30\,\mathrm{W\,m^{-2}}$, we have $h_q = 80\,\mathrm{cm}$.

In sea ice models the oceanic heat flux is normally fixed and often it has been used as a tuning factor. *Maykut and Untersteiner* (1971) employed a constant oceanic heat flux of $6\,\mathrm{W\,m^{-2}}$ to obtain the best-fit equilibrium thickness cycle for multiyear ice in the Arctic Ocean in their classical model. Modelling in the Antarctic seas has indicated that there the heat flux can be one order of magnitude larger. Thus the ice growth may there reach the equilibrium solution (2.28).

Sea ice has not a definite melting point but always warming includes dilution of brine by melting of ice at brine pocket boundaries. In the beginning of the melting season ice is nearly isothermal with temperature close to $0^\circ\mathrm{C}$. Then there is essentially no conduction, and melting can be examined as a process where thickness decreases by melting at the boundaries and by growth of voids in the

interior by solar radiation. Expressing the void volume as thickness equivalent, n, we have:

$$\begin{aligned} \rho L \frac{dh}{dt} &= -(Q_n + Q_w), \quad Q_n \geq 0 \\ \rho L \frac{dn}{dt} &= \lambda Q_{s+} = \lambda(1-\alpha)\gamma e^{-\lambda z} Q_s \end{aligned} \tag{2.29}$$

The net ice volume is $h - n$. At the top surface the snow melts first, then the ice. Snow protects the ice cover due to its high albedo and small optical depth. Thus the internal deterioration starts up only after snow has melted. Internal melting gives rise to structural defects and once the porosity of the ice reaches 0.4–0.5 the ice cannot bear its own weight and breaks into small pieces into the surface water. Then there is a rapid increase in the rate of melting. As an approximation, all melting can be included in the ice thickness when defined as ice volume per unit area, $h^* = h - n$:

$$\frac{dh^*}{dt} = -\frac{1}{\rho L}[Q_n + Q_w + (1-\alpha)\gamma(1 - e^{-\lambda h^*})Q_s], \quad Q_n \geq 0 \tag{2.30}$$

Melting is almost independent of the thickness of ice and dictated by the length of melting season. A heat flux of $30\,\mathrm{W\,m^{-2}}$ would melt the ice vertically by $1\,\mathrm{cm\,day^{-1}}$, and such levels are observed commonly for the net radiation flux in polar summer.

Melting of sea ice takes place also laterally when there is open water between ice floes. Solar radiation is absorbed in leads, and the heat is further transferred to ice floes at their horizontal boundaries. This enhances the solar energy transfer since albedo of water surface is much lower than albedo of ice or snow surface. In addition to influencing the floe size distribution, lateral melting decreases ice compactness.

Consider an ice field of compactness $A < 1$ consisting of uniform floes with thickness h. By simple geometry it is seen that the net energy absorption in leads, Q_n, melts lateral boundaries to decrease the compactness as:

$$\frac{dA}{dt} = -\frac{1}{2} \cdot \frac{Q_n}{\rho L h}(1 - A) \tag{2.31}$$

If the factor $\gamma = Q_n/(2\rho L h)$ is constant, the solution is $A = 1 - (1 - A_0)e^{\gamma t}$. Thus the ice compactness decreases to zero exponentially in time $t = -\gamma^{-1}\log(1 - A_0)$. For $Q_n = 100\,\mathrm{W\,m^{-2}}$ and $h = 1\,\mathrm{m}$, we have $t = 48$ days. In fact, along with lateral melting the ice is melting also vertically, h decreases, and rate of compactness decrease becomes even more accelerated.

Example For a simple illustrative case for the floe size, consider a sea ice field of area S consisting of uniform circular floes with thickness h and diameter d. The energy absorbed by leads is consumed to lateral melting at the floe boundaries and decrease of floe size:

$$Q_n(1 - A)S = -\rho L h N \pi d \frac{\dot{d}}{2}$$

where N is number of floes. Since $AS = N\pi(\frac{1}{2}d)^2$, we have

$$\frac{\dot{d}}{d} = -\frac{1 - A}{2A} \cdot \frac{Q_n}{\rho L h}$$

For $A = \frac{1}{2}$, $h = 1\,\mathrm{m}$ and $Q_w = 100\,\mathrm{W\,m^{-2}}$, the floe size decreases by 1.4% per day. Full integration of this equation needs integration of the compactness (Eq. 2.31) simultaneously, here we get just idea of the scale.

Finally, analytic growth and melting models can be combined for the equilibrium multiyear ice thickness. In one winter sea ice grows to 0.5–2 m thickness while in summer ice melts up to 1 m. Where the summer melt is less than the first year's growth, multi-year ice develops. This is the case in the Central Arctic Ocean and in places in the Southern Ocean, mainly in the Weddell Sea.

Zubov's model is taken as the basis. The thickness of ice after the n'th summer is

$$h_n = \sqrt{h_{n-1}^2 + 2h_{n-1}\delta + \delta^2 + aS} - \delta - \Delta h, \quad n \geq 1 \tag{2.32}$$

where Δh is the summer melting, which is determined by the radiation balance and oceanic heat flux; here we take $\Delta h \approx$ constant (independent of ice thickness). At equilibrium, $h_{n+1} = h_n = h_e$, where h_e is the equilibrium thickness of multi-year ice:

$$h_e = \frac{aS - (\Delta h)^2}{2\Delta h} - \delta \tag{2.33}$$

The condition of multi-year ice is trivial: $h_1 > \Delta h$. For $h_1 = 2\,\mathrm{m}$, $\Delta h = \frac{1}{2}\,\mathrm{m}$ and $\delta = 10\,\mathrm{cm}$, we have $h_e = 3.55\,\mathrm{m}$, but changing the summer melt to 1 m gives us $h_e = 1.3\,\mathrm{m}$, illustrating the high sensitivity to the equilibrium thickness to summer melt.

2.3.4 Numerical modelling of ice thermodynamics

Development of numerical models of sea ice thermodynamics began in the late 1960s. Maykut and Untersteiner (1971) presented a model for congelation ice temperature and thickness based on full heat conduction law. A simplified version was prepared by Semtner (1976) for climate simulations, and snow-ice models were added by Leppäranta (1983) and Saloranta (2000). In numerical modelling the temperature profile and resulting heat flow is solved in a dense grid across the ice sheet. Compared with the analytical models, more realistic boundary conditions can be applied and the thermal inertia of the heat flow through the ice can be included. In these models the salinity of the ice is prescribed and together with the temperature determines the brine volume; a full temperature-salinity model for sea ice has not yet been developed.

Numerical models of sea ice thermodynamics are vertical since the heat transfer is slow to reach any significant distance in the horizontal directions. The equation for heat conduction becomes:

$$\frac{\partial}{\partial t}(\rho c T) = \frac{\partial}{\partial z}\left(\kappa \frac{\partial T}{\partial z} - Q_{s+}\right) \tag{2.34a}$$

$$\textit{Surface}: \kappa \frac{\partial T}{\partial z} = Q_n + m(T)\rho L \frac{dh}{dt} \tag{2.34b}$$

$$\textit{Bottom}: T = T_f, \quad \kappa \frac{\partial T}{\partial z} = Q_w + \rho_i L \frac{dh}{dt} \tag{2.34c}$$

where $m(T) = 1$ for $T = T_f$ or 0 otherwise. Equations (2.34b–c) state that the heat fluxes are continuous through the upper and lower surfaces: conduction into ice equals external heat flux plus heat release or take-up due to phase changes. In the presence of slush, snow-ice forms in the upper layers in a similar way and since slush contains ice crystals less latent heat is released. The thermal properties of sea ice depend on the brine volume, which depends on temperature and salinity (see Maykut and Untersteiner, 1971). Since flow of brine and consequent desalinization depends on its volume, the temperature and salinity of sea ice constitute a coupled problem.

The exchange of mass and heat with the atmosphere and the incoming solar radiation define the boundary conditions at the surface of the ice-sheet. They are given, respectively, as

$$h' = P - E \tag{2.35a}$$

$$Q_n = (1 - \alpha)(1 - \gamma)Q_s + Q_{nL} + Q_c + Q_e + Q_P \tag{2.35b}$$

where P is precipitation and E is evaporation, Q_{nL} is net longwave radiation, Q_c and Q_e are sensible and latent heat fluxes, and Q_P is the heat provided by precipitation. Estimation methods for these heat fluxes are presented, e.g., by Makshtas (1984), Andreas (1998) and Curry and Webster (1999).

Numerical congelation ice models have a passive snow layer, and they were later extended to include an interacting snow model (Leppäranta, 1983; Saloranta, 2000; Shirasawa *et al.*, 2005). The sea ice–snow model consists of four types of layer: snow, slush, snow-ice and congelation ice. These layers are interacting: snow accumulation creates slush and snow-ice depending on the total thickness of ice, while the growth and decay of congelation ice depend on the snow and slush conditions. The snow layer needs its own model. The thickness of snow decreases due to three different reasons: surface melting, compaction, and formation of slush, which further transforms into snow-ice.

The outcome of the Maykut and Untersteiner (1971) model for the annual cycle is shown in Figure 2.14. The equilibrium thickness is sensitive to three factors: oceanic heat flux, snow accumulation and albedo. With zero oceanic heat flux the equilibrium thickness was doubled as compared with the standard case of 6 $\mathrm{W\,m^{-2}}$. The role of snow is protective since large amounts of snow reduce the summer melt. In the Maykut-Untersteiner model the summer albedo was kept at 0.64, and it was shown that lowering that to 0.44 melted all ice in summer from the Arctic Ocean.

Shirasawa *et al.* (2005) used the congelation ice–snow-ice model in the Sea of Okhotsk (Figure 2.15). Offshore Sakhalin the result was very good but it was worse for offshore Hokkaido, where the ice is thinner. This is a general problem in sea ice thermodynamics that thin ice is difficult to simulate. However, the result in Hokkaido was useful and showed the high sensitivity of ice thickness and stratigraphy to amount and timing of snowfall.

In sea ice dynamics models the grid size is 10–100 km, and thermodynamics act independently in the grid cells. In purely dynamical models thermodynamics is ignored, which is often a reasonable assumption in short-term simulations. The critical limit is the time scale when open water has reached a significant thickness to

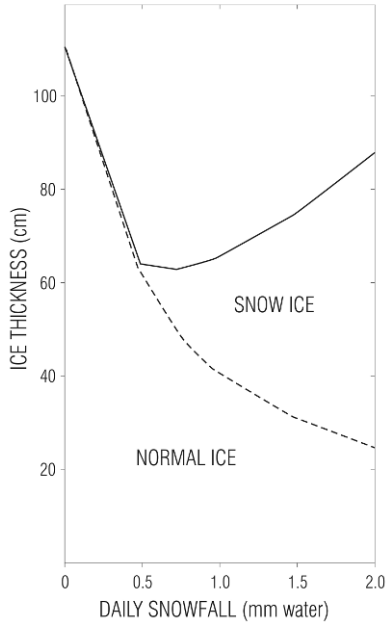

Figure 2.13 The proportions of congelation ice and snow-ice as a function of snow accumulation history for conditions in Oulu, northern Baltic Sea. Air temperature follows climatology and snowfall comes at a fixed rate shown in the *x*-axis.
From Leppäranta (1983).

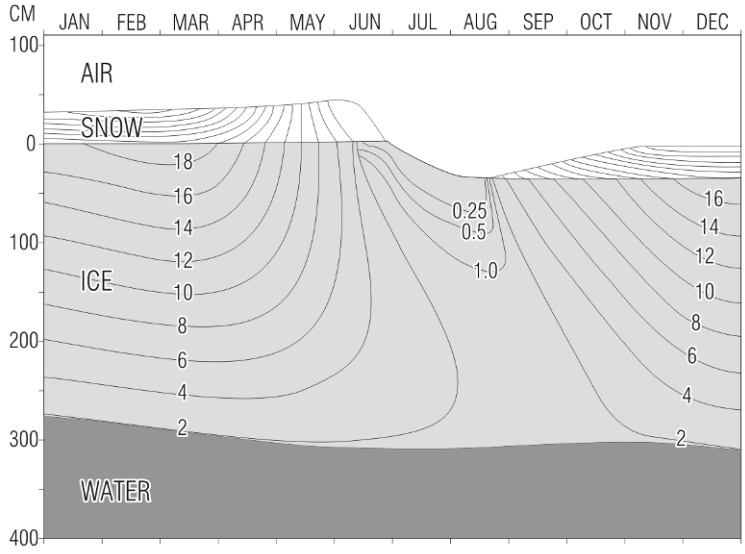

Figure 2.14 Annual cycle of ice temperature (isotherms inside ice and snow in °C) and thickness (scale on the left, cm) of multi-year ice at the equilibrium thickness.
Redrawn from Maykut and Untersteiner (1971).

contribute into the strength of the ice cover. The magnitude of this thickness ranges from 10 cm in SSIZ to 50 cm in the Central Arctic Ocean; using Zubov's model we can see that the corresponding time scale is 3 days in the SSIZ if $T_a = -10°C$ or 15 days in the Central Arctic if $T_a = -20°C$. Formally, when thermodynamics is taken into account, a *growth rate function* $\Phi = \Phi(t, h)$ is added into the ice conservation law, with melting specified by negative growth rates. This growth rate can be taken from climatology or produced using a thermodynamic model, whose complexity level is a question of choice. Thermal growth has the tendency of smoothing the ice field since thin ice grows faster than thick ice, but melting, first of all due to the patchiness of albedo, works to spread the thickness distribution.

2.4 THICKNESS OF DRIFT ICE

2.4.1 Mechanical ice growth

Sea ice thickness is characterized by a very large variability in space and time due to thermal and mechanical processes. The thickness range extends from zero, defining open water as "ice of zero thickness" up to as much as 50 m in the largest pressure ridges. Sea ice thickness is an irregular field and, because of fracturing and new ice growth in leads, it may have discontinuities. In the continuum approach, certain

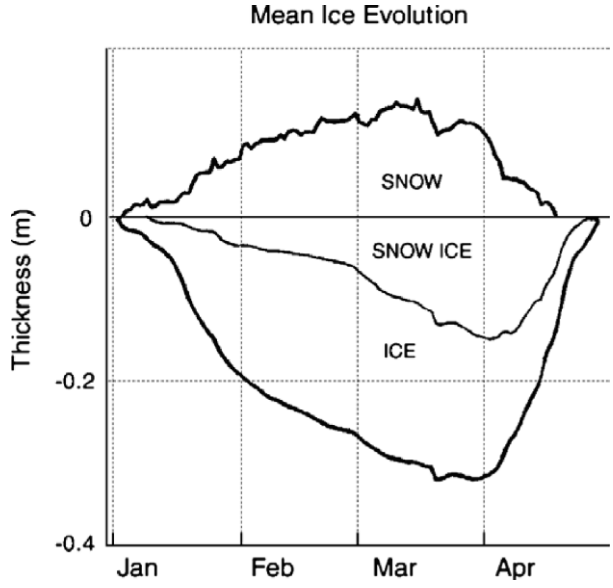

Figure 2.15 Mean modelled thickness of snow, snow-ice and congelation ice layers in Saroma-ko lagoon off in Hokkaido. Snow is shown above the zero line, snow-ice and congelation layers below the zero line.
From Shirasawa *et al.* (2005).

statistics of the thickness field, such as mean thickness, are considered for each continuum particle; these statistics are assumed to be smooth, as required by the theory. In the previous section thermodynamics was considered, and in this section the picture is completed with the presentation of sea ice thickness evolution as a result of mechanics.

Sea ice, which has formed mechanically from broken, thermally grown ice is called *deformed ice*. At a smaller scale, the thickness of deformed ice may vary a lot. A good illustration is provided by upward-looking submarine sonar data (Figure 2.16). Most of the thickness section is quite heavily deformed, which is typical for the Greenland Sea ice conditions. In this section ridge keels penetrate 10–20 m beneath the sea level (there are five ridge keels for this 2-km section). Rothrock (1986) shows a thickness section from the Beaufort Sea with a correlation length scale of the order of 1 km; the standard deviation was 2.4 m and the average was 3 m.

Mechanical deformation produces ice types with a range of thicknesses. Most of the variability in sea ice thickness is caused by mechanics, since pressure ridges form in time scales of several hours. Mechanical thickness changes are asymmetric in that, while mechanical increase of ice thickness takes place, existing deformed ice is not undone mechanically but may disappear only because of melting. This also means that transforming kinetic energy into potential energy in deformation is mechanically irrecoverable. Thus pressure ice build-up while increasing the volume and strength of the ice does not lead to returning forces, in contrast to ocean dynamics.

Thin ice usually undergoes rafting in compression (Figure 2.17). A theoretical formula for the maximum thickness of rafting ice is (Parmerter, 1975):

$$h_{rf} = \frac{14.2(1-\nu^2)}{\rho_w g}\frac{\sigma_t^2}{Y} \tag{2.36}$$

where σ_t is the tensile strength of the ice sheet, a representative value being 0.65 MPa (Mellor, 1986). This gives $h_{rf} = 15$–20 cm. In single rafting the local thickness is doubled. Several layers of rafted ice have been documented (Palosuo, 1953;

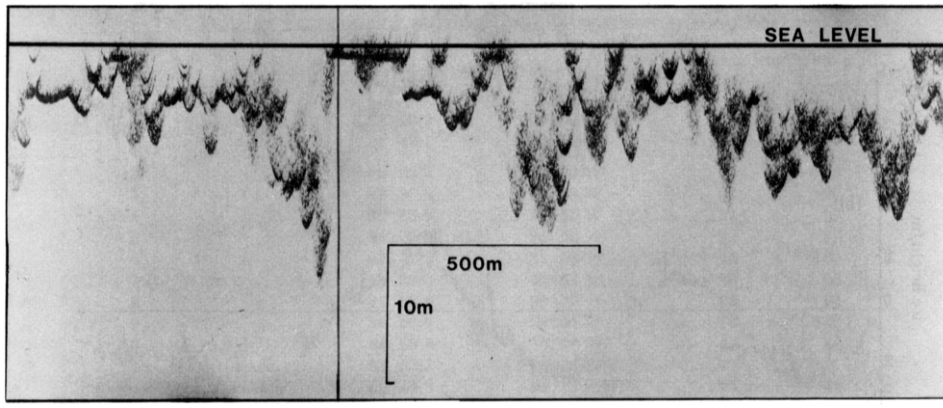

Figure 2.16 A section of ice draft profile in the Greenland Sea from submarine sounding. Reproduced from Wadhams (1981), with permission from the Royal Society of London.

Bukharitsin, 1986). As the ice thickness increases, bending moments as a result of overriding become so large that small pieces break off and start to form hummocks and ridges. When thin ice is compressed against thick ice (in particular, at the fast ice boundary), jammed brash ice barriers form. Contrary to other deformed ice types, these barriers may loosen when the compressive force ceases. Working with predominantly very thin ice, the rafting process would need particular consideration.

Hummocking accumulates ice blocks into layers several times the thickness of the original ice sheet (Figure 1.2a). The thickest forms of drift ice, ridges, may be up to 50 m thick. Fresh hummocks and ridges contain voids (20–40%) between the ice blocks. In cold conditions a consolidated layer grows down from the sea surface level. Thus the ice volume is 0.6–1.0 times the thickness, depending on the degree of consolidation.

Example (*piling*) Piling uniform-sized balls on top of each other results in open and closed locked packings of $\pi/6 \approx 0.52$ and $\sqrt{2} \cdot \pi/6 \approx 0.74$, respectively (corresponding porosities are 0.48 and 0.26). Experience shows that, when piling chopped firewood by randomly throwing one piece on top of each other, porosity will be about 1/3. The closed packing of balls and random firewood piling are well within the range of the observed porosities of new hummocks and ridges.

2.4.2 Measurement methods

To obtain thickness information is very difficult. A lot of effort has been put into this problem in sea ice remote sensing (e.g., Rossiter and Holladay, 1994; Wadhams, 2000). A good solution still does not exist – a major barrier to the progress of knowledge in drift ice dynamics. The basic techniques of sea ice thickness mapping are listed in Table 2.3.

Drilling is the traditional way of determining ice thickness, a direct measurement but not feasible for mesoscale or large-scale monitoring. One specific methodology for thickness mapping is recording from a ship (ice-breaker) the thickness of

Table 2.3 Methods for sea-ice thickness measurement.

Method	Quality	Comments	Reference
Drilling	Excellent	Laborious	Traditional
Submarine sonar	Good	Access problems	Williams *et al.* (1975)
Bottom-moored sonar	Good	Non-real-time	Vinje and Berge (1989)
AEM	Good	Resolution ~ flight altitude	Kovacs and Holladay (1990)
Thermal mapping	Fair	Thin ice OK	Steffen and Lewis (1988)
Airborne laser	Fair	Sea ice ridges OK	Ketchum (1971)
GPR	Poor	Problems with brine	Rossiter *et al.* (1980)
SAR	Poor	Ice types only	Kwok *et al.* (1992)
Passive microwave	Poor	Ice types only	Gloersen *et al.* (1978)

overturned ice blocks (Overgaard *et al.*, 1983). Upward-looking sonar systems are considered the best method for ice thickness mapping by remote sensing. They measure the draft, which provides a very good estimate for total thickness. They are, however, restricted by their high instrumental and logistics costs, and the unavailability of real-time data. Submarine sonars have been routinely used since the 1950s (Lyon, 1961) but their data are normally classified (Figure 2.16 shows an example). Bottom-moored sonars were developed in the 1980s for ice thickness mapping (Vinje and Berge, 1989).

The airborne electromagnetic method (AEM), originally developed for ore prospecting and geological surveys, was introduced in the late 1980s for sea ice thickness mapping (see Rossiter and Holladay, 1994). By emitting electromagnetic fields at frequencies of 1–10 kHz, eddy currents are generated in the conductive seawater. These currents generate a secondary electromagnetic field, and, measuring this field at the receiver, the distance to seawater can be determined. Measuring the distance to the sea ice surface by an altimeter, the sea ice thickness is obtained. AEM is a logistically feasible way for reliable and quick ice thickness mapping. It also provides line data with a resolution of the order of the flight altitude (30–100 m). Thus ridges can be identified for their total cross-sectional area but not for the geometric structure. The accuracy of results depends on the inversion model used (Figure 2.18),

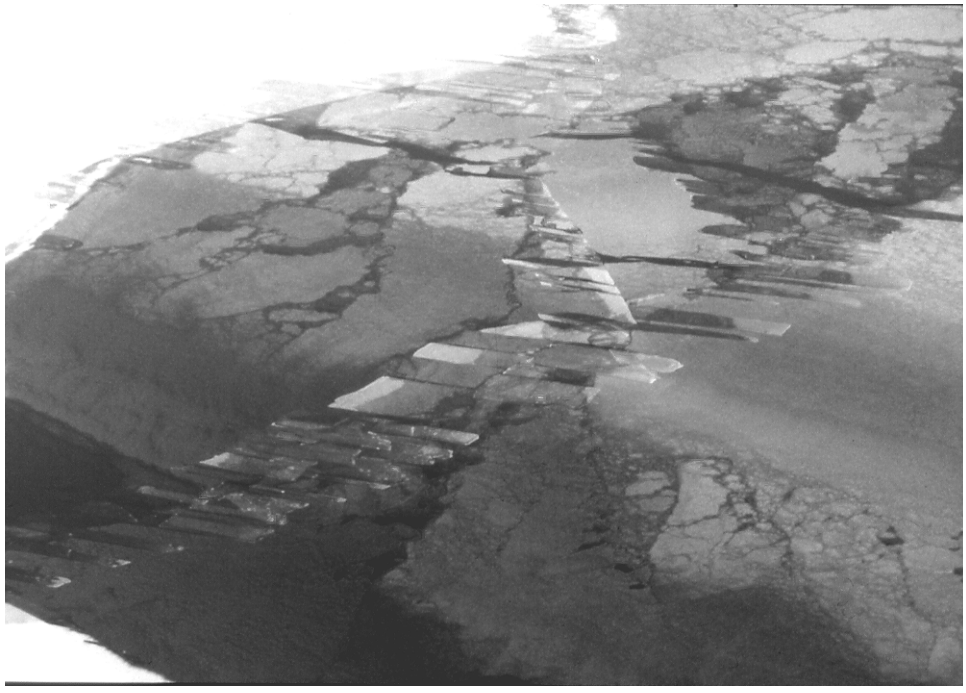

Figure 2.17 Thin ice sheets undergo rafting in compression. The width of the interlocking fingers in the picture varies between 1 and 10 m.

since by adding layers a more realistic conductivity distribution can be taken for the ice. Surface-based or shipborne EM systems have also been introduced (Haas, 1998).

Thermal infrared mapping can be applied to sea ice mapping in cold weather because the surface temperature of sea ice and the eventual snow cover on top depend on the structure and thickness of the ice and snow. It works well for ice thinner than about 50 cm when the air temperature is less than 5°C (Steffen and Lewis, 1988; Leppäranta and Lewis, 2007). Airborne laser profilometers give the upper surface topography (quite widely used since 1970). In principle, surface elevation can be interpreted for total ice thickness using Archimedes' law, but the measurement accuracy and snow cover cause severe problems. However, sea ice ridges are shown in surface topography profiles and constitute the principal aim of laser surveys.

Microwave sea ice mapping is carried out by ground-penetrating radar (GPR), synthetic aperture radar (SAR), and the (passive) radiometer. They are widely used for sea ice mapping but provide only poor results for ice thickness (Rossiter and Holladay, 1994; Kwok *et al.*, 1998; Wadhams, 2000; Karvonen *et al.*, 2005). Radar signals cannot penetrate sea ice because of brine and seawater inclusions, and the direct connection between ice thickness and backscatter is weak. SAR can detect two to four nominal ice types: the most promising is ridged ice, because piled-up ice blocks give strong backscatter. Microwave radiometers (10–100 GHz) can differentiate between open water, first-year ice and, to some degree, multi-year ice (Gloersen *et al.*, 1978; Kondratyev *et al.*, 1996). On the global scale they are by far the most used system for collecting sea ice information (see Figure 2.5).

A particular technique is ship-borne remote sensing. It is limited by the ship's tactical navigation to find the best route and it is therefore biased toward smaller thicknesses; however, the advantages are simplicity and low costs. The methods have included photography and video recording of ice blocks turning as the ice is broken (Overgaard et al. 1983; Shimoda *et al.*, 1997; Lu and Li, 2009), oblique-view laser profilometry (Leppäranta and Palosuo, 1981) and EM surveys.

It is clear that no single method is sufficient for ice thickness mapping; rather, a combination of instruments is needed to cover the whole range from 0 m to 50 m thicknesses. Satellite-derived thickness information results in poor quality, as it is only based on the thermal method or microwaves, both of which are of limited use. In 2010 ESA launched satellite *CryoSat 2*[6], which is designed for mapping thickness of sea ice and glaciers (`http://www.esa.int/esaLP/LPcryosat.html`). The measurement accuracy for polar sea ice is claimed to be good enough to monitor annual variations in sea ice thickness. *CryoSat-2* carries a sophisticated radar altimeter called SIRAL (Synthetic Aperture Radar Interferometric Radar Altimeter). The system measures the freeboard, and the accuracy of the resulting mean thickness is, according to ESA, 1.6 cm for Arctic sea ice areas in the scale of 10^5 km^2 and 0.17 cm in the Antarctica in the area scale of 10^6 km^2. These accuracies are better by a factor of 2–3 as specified by the scientific requirements.

[6] The trial with *CryoSat 1* in 2005 resulted in destruction of the satellite due to launch failure.

2.4.3 Ice thickness distribution

In sea ice dynamics – as well as in sea ice geophysics and engineering in general – sea ice thickness is the primary ice property of ice fields. It determines the volume and strength of ice cover, and is a key ice parameter in estimating ice loads on structures and navigation conditions. The mean sea ice thickness in continuum length scales is 2–8 m in the Central Arctic Ocean. It is lower in the Eurasian Shelf and at its highest off northern Greenland and the Canadian Archipelago (Figure 2.19). Distribution is strongly influenced by the drift of ice. Without dynamics the thickness would be more or less symmetric around the North Pole, but due to ice transport it is lowest (about 2 m) on the Siberian Shelf and 3 m or more in the Beaufort Sea. The highest thicknesses, averaging 8 m, result from the mechanical deformation of ice. In the seasonal sea ice zone the mean thicknesses range in $\frac{1}{2}$–2 m. In the Antarctic sea ice thicknesses are much less than in the Arctic. According to a large ship-borne data set, the long-term mean and standard deviation of total sea ice thickness is reported as 0.87 ± 0.91 m, which is 40% greater than the mean thickness of undeformed ice, 0.62 m (Worby *et al.*, 2008). The correlation length scale was 100–300 km.

In the continuum length scales sea ice thickness is presented using a thickness distribution (Thorndike *et al.*, 1975). With this approach it is possible to include the large thickness variability in the analysis and modelling of ice dynamics. Let $\underline{h} = \underline{h}(x, y; t)$ stand for the actual ice thickness and h represent the ice thickness as the distribution variable. Recalling the ice function I in Eq. (2.4) we have $1 - I(h) = 1$ if $\underline{h} \leq h$ or 0 if $\underline{h} > h$. In a region Ω, the area of ice thinner than or equal to h is:

$$S(h) = \int_{\Omega} [1 - I(h)] \, \mathrm{d}\Omega \tag{2.37a}$$

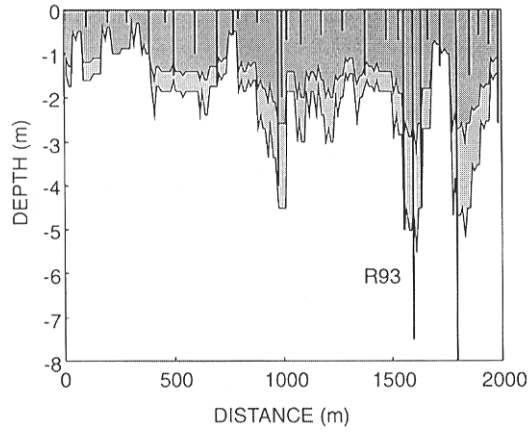

Figure 2.18 AEM calibration for ice thickness in the Baltic Sea, March 1993. The vertical bars show drilling data, dark and light-shaded areas show inversions with one- and two-layer models, respectively (the footprint is 100 m).
From Multala *et al.* (1996).

Thus $S(0)$ is the area of open water and $S(\infty)$ is the total area of Ω. The normalized form of the distribution:

$$\Pi(h) = \frac{S(h)}{S(\infty)} \tag{2.37b}$$

is the spatial ice thickness distribution, analogous to the probability distribution[7]. The derivative (in the generalized sense) of Π, $\pi(h) = \mathrm{d}\Pi/\mathrm{d}h$, is the spatial density of the ice thickness. *Note*: the thickness distribution was originally (Thorndike *et al.*, 1975) chosen continuous from the right (i.e., $S(h)$ equal to the area of ice thinner than h); here it is continuous from the left (i.e., $S(h)$ equal to the area of ice thinner than or equal to h). The current way is also common in probability theory; the difference is academic, though.

The thickness distribution is not continuous[8] everywhere since part of the spatial density mass is concentrated in open water and in homogenous ice patches. These discontinuities can be mathematically handled using the delta function δ and Heaviside function H:

$$\delta(s) = 0, \quad \text{if } s \neq 0, \quad \text{and} \quad \int_{-\infty}^{\infty} \delta(s) f(s) ds = f(0) \tag{2.38a}$$

$$H(s) = \begin{cases} 0, & s < 0 \\ 1, & s \geq 0 \end{cases} \tag{2.38b}$$

where f is for any integrable function. They are connected by the generalized derivative:

$$\frac{dH}{ds} = \delta(s) \tag{2.38c}$$

The spatial (cumulative) distribution function and density can be written as sums of discrete parts and continuous parts:

$$\Pi(h) = \sum_k \pi_k H(h - h_k) + \Pi'(h) \tag{2.39a}$$

$$\pi(h) = \sum_k \pi_k \delta(h - h_k) + \pi'(h) \tag{2.39b}$$

where π_k's are the probabilities of discrete thicknesses h_k, $k = 0, 1, \ldots, \Pi'$ is the continuous component of the distribution, and $\pi' = \mathrm{d}\Pi'/\mathrm{d}h$.

The thickness distribution has the following mathematical properties:

(i) $\Pi(0) = 1 - A$ and $\Pi(\infty) = 1$ by definition.
(ii) The first moment is the mean ice thickness.
(iii) The second moment is proportional to the mean potential energy of the ice (see Eq. 2.2).

[7] Analogous but physically dissimilar; there is no random field embedded, the distribution describes the variability of the real field of ice thickness – as in mechanics of rigid bodies.
[8] For continuity, the left and right limits must exist and be equal.

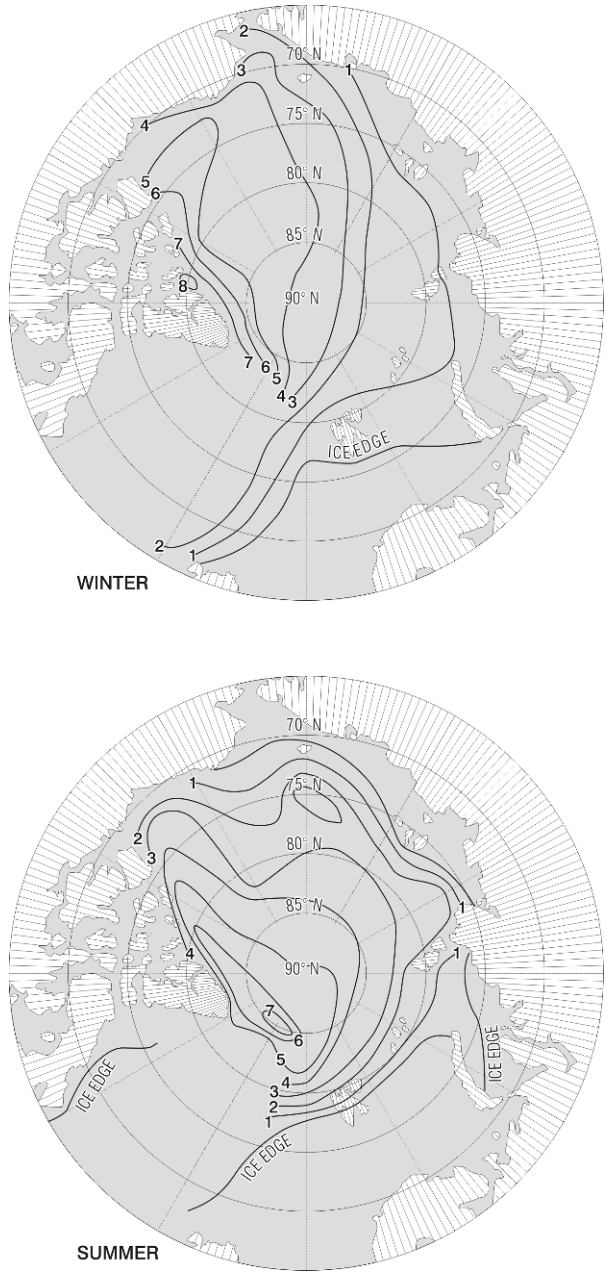

Figure 2.19 Mean sea ice draft in the Arctic Ocean based on submarine data. Since Archimedes' law states that 89% of the ice sheet is beneath the sea surface, the mean sea ice thickness is obtained by multiplying these draft numbers by 1.12.
Reproduced from Bourke and Garret (1987), with permission from Elsevier.

There is no simple general form for the distribution function because of the very large space-time variability of its shape, and therefore discrete histogram approximations are used. However, the upper tail of the spatial density containing deformed ice drops to zero exponentially (Wadhams, 1998). The thickness distribution includes both undeformed and deformed ice but ignores spatial information about the structure of drift ice. Figure 2.20 shows ice thickness distributions from both polar regions. The multi-year peak is well developed only in the Arctic Ocean, and there is much less deformed ice in Antarctica.

2.5 SEA ICE RIDGES

Sea ice ridges are a particular form of deformed ice or pressure ice (Figure 2.21). They are the thickest ice formations, typically 5–30 m, and over large areas their volume may account for up to about one-half of the total ice volume. In sea ice dynamics, ridging is the main sink of kinetic energy in deformation due to friction and production of potential energy (Rothrock, 1975a). Ridges are important hydrodynamic form drag elements at the air–ice and ice–water interfaces. In ice engineering, ridges are of deep concern because (i) they are connected with the highest ice loads on structures within first-year ice fields, (ii) they scour the sea bottom, (iii) they influence shipping conditions, and (iv) they influence on-ice traffic conditions. *In situ* field studies on the structure of ridges are made by drilling, diving and sonar, while their spatial statistics are mapped by remote-sensing methods, primarily airborne laser profilometer, SAR, and submarine upward-looking sonar.

2.5.1 Structure of ridges

Detailed investigations of the structure of sea ice ridges commenced in the 1960s from the needs of polar ocean engineering (Palosuo, 1970; Kovacs, 1971; Weeks *et al.*, 1971). The top part of a ridge is called *the sail* and the lower part is called *the keel;* in the keel there is a *consolidated zone*, which grows downward from the water surface level as the ridge ages. In the sail and lower keel the ice blocks are loose or weakly frozen together. A simple structural model of ridges (Figure 2.21) consists of triangular keel and sail, described by the keel depth h_k, sail height h_s, slope angles φ, and porosity ν; $\varphi \approx 30^\circ$ (keel) or 20° (sail) and $\nu \approx 0.25$ (e.g., Timco and Burden, 1997; Kankaanpää, 1998). The cross-sectional volumes of keel and sail are $h_k^2 \cot \varphi_k$ and $h_s^2 \cot \varphi_s$. A more general model would have a trapezoidal keel.

The structure of a ridge undergoes continuous evolution due to freezing, melting and erosion, becoming smoother with time (Figure 2.22). Erosion of roughness features smoothes the external geometry, and in the interior consolidation takes place in the keel. Contacts freeze between ice blocks, first releasing the latent heat to warm ice blocks in a fresh ridge. The capacity of the blocks to absorb latent heat is

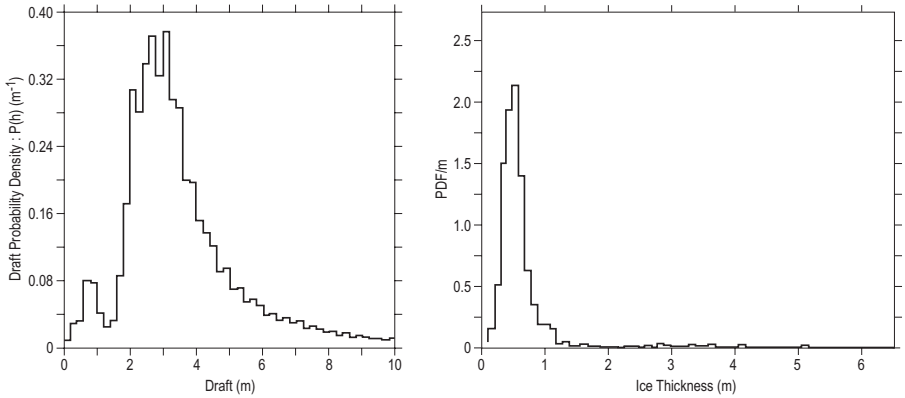

Figure 2.20 Observed ice thickness distributions. Left: Fram Strait (Wadhams, 1980a). Right: Antarctica, Atlantic sector (Wadhams *et al.*, 1987).

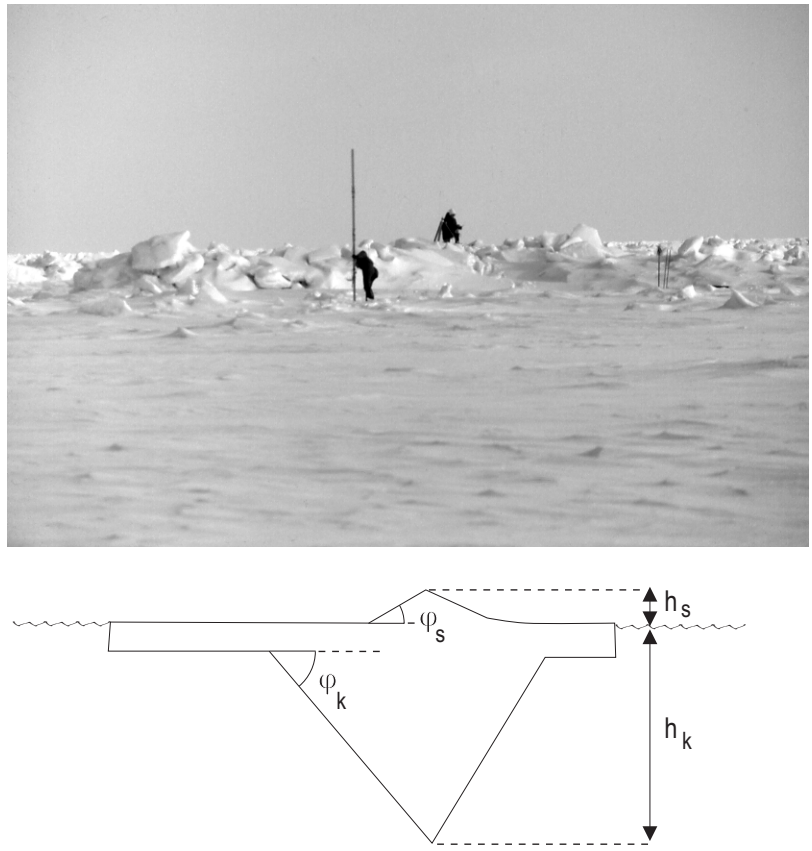

Figure 2.21 An ice ridge shown in a field photograph (Baltic Sea, March 1988) and in a schematic cross-sectional diagram.

not large, and for further consolidation the latent heat must be conducted to the atmosphere. By this way, the consolidation front progresses downward inside the ridge, and the growth rate can be approximated using the Zubov model (see Section 2.3), with the modification that latent heat released in consolidation equals νL. The solution is therefore for the thickness of the consolidated layer:

$$h_F = \sqrt{a^2 \nu^{-1} S + \delta^2} - \delta \tag{2.40}$$

That is, asymptotically, as $h_F \gg \delta$, the thickness of the consolidated layer grows $\nu^{-1/2} \approx 2$ times faster than undeformed ice. This has been well documented in observational data (Leppäranta and Hakala, 1992). Applying equilibrium thickness results (Eq. 2.33) to multi-year ridges, a theoretical limit thickness would be about 15 m as long as there are ice blocks to take into consolidation. But when the blocks are all taken into the solid ridge or melted, the thickness would start to come down toward the equilibrium thickness of undeformed ice. The whole cycle would take, however, several decades, and therefore thick, solid, old multi-year ridges are occasionally observed in the Central Arctic Ocean.

Ice ridges float according to the Archimedes' law (see Eq. 2.1). The ratio of keel depth to sail height $\gamma = h_k/h_s$ is obtained from:

$$(\rho_w - \rho) h_k^2 \cot \varphi_k = \rho h_s^2 \cot \varphi_s \tag{2.41}$$

We have $\gamma = 2.8$ for $\varphi_k = \varphi_s$ and $\gamma = 3.5$ for $\varphi_k = 30^\circ$, $\varphi_s = 20^\circ$. According to observations, for multi-year ridges $\gamma \approx 3$ but for first-year ice ridges $\gamma \approx 4$–5 (Wright *et al.*, 1978). The latter case comes from the keel being steeper than the sail. Wittman and Schule (1966) presented a triangular keel model with $\gamma \approx 3.3$ based on field data. Once the sail height is known, the total cross-section of a ridge can be estimated as $R = k h_s^2$ where the coefficient k represents all structural parameters. For the Baltic Sea, according to Leppäranta and Hakala (1992), $k \approx 17$.

A physical limitation exists for ridge growth (Parmerter and Coon, 1972; Hopkins and Hibler, 1991). When a ridge has grown to a certain vertical size, the ice sheet is too weak to penetrate into the ridge, for further growth. It breaks in front of the ridge, producing lateral growth. This limiting size mainly depends on the thickness of the parent ice sheet (very few ridges grow to this size). The record ridge sizes come from the Beaufort Sea (Wright *et al.*, 1978): a floating ridge with a sail height of 12 m and a keel depth of 45 m, and a grounded ridge with a sail height of 18 m.

In shallow areas where the sea depth is less than the keel depth, grounding takes place and ridges anchor to form fixed ice islands. This is typically observed at the landfast ice boundary. Grounded ridges serve as tie points to the ice and therefore help the fast ice boundary to extend farther away from the coast. Grounded ridges, when moving, scour the ocean bottom, and the keel may penetrate deep, depending on the bottom material (Blondel and Murton, 1997). As a consequence, cables and pipes laid on the floor of shelf waters must be buried deep enough to avoid damage from scouring keels.

2.5.2 Statistical distributions of ridge size and occurrence

Ridges give an impressive feature to the drift ice landscape (Figure 2.23). The spatial distribution of ridging is described in terms of their size and occurrence. The first occurrence data were counts made in reconnaissance flights resulting in a typical level of 5–10 ridges per km, with a maximum of 20 ridges per km (Wittman and Schule, 1966). At present, ridges are usually mapped using airborne laser profilometers for sails (Ketchum, 1971; Hibler *et al.*, 1972; Lewis *et al.*, 1993) and using upward-looking sonar for keels (Williams *et al.*, 1975; Vinje and Berge, 1989).

A cut-off size, h_c, needs to be introduced, since the size of the chosen ridges must be well above the noise level of the measurement system. Also sails should not be mixed with snowdrifts. The cut-off sizes have been 1 m (or 3 feet $\approx$ 0.9 m) for sails and 5 m for the keels in the polar oceans, somewhat lower in smaller subpolar basins

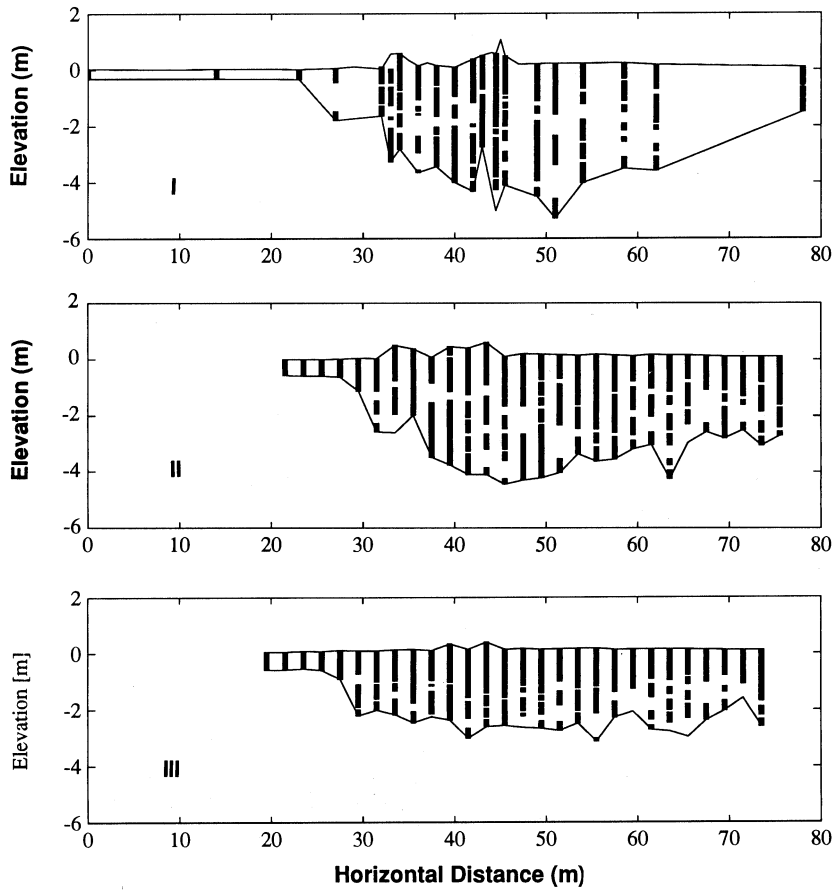

Figure 2.22 The evolution of the cross-sectional profile of one ridge near Hailuoto island, Baltic Sea, winter 1991 (Leppäranta *et al.*, 1995).

such as 0.4 m in the Baltic. Independent sails or keels are taken from observed surface profiles using the Rayleigh criterion: ridges are taken as the local maxima, which are greater than the cut-off height and between which there is a local minimum with elevation less than half of these maxima. The cut-off is more a parameter related to observational technology than to real ice. Visual counts have given about the same number of sails as laser profilometer measurements. This confirms that the cut-off is well tuned to reflect how the ice field looks from above, a situation that is also true of the concept of the significant wave height of wind-driven surface waves.

Ridge size

Sail heights or keel depths follow the exponential distribution:

$$p(h*; h_c, \lambda) = \lambda \exp[-\lambda(h* - h_c)], \quad h* \geq h_c \tag{2.42}$$

where $h*$ represents the sail height or keel depth, and λ is the distribution shape parameter. The mean size is simply $h_c + \lambda^{-1}$ and the standard deviation is λ^{-1}. This distribution was first proposed by Wadhams (1980a) for the Arctic Ocean, and it has been confirmed several times, for sails in the Baltic Sea (Leppäranta, 1981b; Lewis *et al.*, 1993) and in the Antarctic (Weeks *et al.*, 1989; Granberg and Leppäranta, 1999), and for keels in the Arctic by Wadhams and Davy (1986). The first size distribution was proposed by Hibler *et al.* (1972) who arrived at a probability density proportional to $\exp(-h_*^2)$.

The statistical background of the size distribution can be based on a certain random hypothesis concerning the probabilities of the different size arrangements (see Hibler *et al.*, 1972). The exponential distribution comes from assuming that all height arrangements yielding the same total sum are equally probable. Such a hypothesis, however, has no clear physical background. Representative values for the mean sail height and keel depth in the central Arctic Ocean are $\tilde{h}_s \approx 1.2$–1.4 m (cut-off 0.9 m) and $\tilde{h}_k \approx 8$–14 m (cut-off 6.1 m) (Hibler *et al.*, 1972). Therefore the parameter λ^{-1} is 0.3–0.5 m for sails and 2–5 m for keels. In the Baltic Sea the mean sail height was 0.5–0.6 m (cut-off 0.4m) in Lewis *et al.* (1993).

Ridge spacing

Spacings between ridges relate in some way to the size of ice floes, and so we expect similar statistical laws to apply to them (see Section 2.2). In fact, the first model for ridge spacings was the exponential distribution (Hibler *et al.*, 1972). It was later replaced by the logarithmic normal distribution (Wadhams and Davy, 1986; Lewis *et al.*, 1993), giving the impression that new ridges would be randomly born at any point between existing ridges. In the seasonal sea ice zone, as in the Baltic Sea, this may be true. However, in the central Arctic Ocean ridges form in leads and, in turn, the birth of ridges therefore follows the distribution of lead spacings and inherits the logarithmic normal form. The fit is in general not excellent, though, and an attempt was made in Lensu (2003) to improve the distribution model by including a

clustering effect in ridging. Representative values for mean ridge spacing are 5–10 km^{-1} in the Central Arctic Ocean and in the Baltic Sea, but with different cut-off sail heights, 0.9 m and 0.4 m, respectively (Hibler *et al.*, 1972; Lewis *et al.*, 1993).

The inverse mean ridge spacing μ is called the ridge density and is equal to the mean number of ridges per length. It depends on the cut-off size. So, assuming the exponential distribution for ridge size, we have:

$$\mu(h_{c2}) = exp[-\lambda(h_{c2} - h_c)]\mu(h_c) \tag{2.43}$$

where h_c is the original cut-off height and h_{c2} is the new one. With regard to the two-dimensional aspects of spacing, deviations from isotropy occur as one would expect (e.g., Mock *et al.*, 1972; Leppäranta and Palosuo, 1983). However, the isotropy has so far been the main working hypothesis. It simply leads from one to two dimensions through (Mock *et al.*, 1972):

$$\frac{L_R}{S} = \frac{\pi}{2}\,\mu \tag{2.44}$$

where L_R is the total length of ridges in the horizontal area S. For anisotropic cases this equation has been found reasonable when using the directionally averaged ridge density parameter.

2.5.3 Ridging measures

The ridge size and spacing distributions can be combined to form a measure of ridging intensity. Two natural measures arise: $\mu\tilde{h}_*$ and $\mu\tilde{h}_s^2$. The first one is dimensionless and describes the sum of sail heights or keel depths per unit length (with sails it is also proportional to the aerodynamic form drag of ridges: Arya, 1973). The second has the dimension of length and is proportional to the mean thickness of ridges, h_R. This quantity and the areal concentration of ridges (S_R/S) are:

$$h_R = \frac{\pi}{2}\,\mu\tilde{R}, \quad \frac{S_R}{S} = \frac{\pi}{2}\,\mu\tilde{b}_R \tag{2.45}$$

where b_R is the ridge width. If only sail data exist, the cross-section and width of ridges are approximated by $R \approx k h_s^2$ and then $h_R = \frac{1}{2}\pi\mu k\tilde{h}_s^2$ and $b_R = 2\gamma h_s \cot\varphi_k$. Hibler *et al.* (1972) used the formula $h_R = 10\pi\mu\tilde{h}_s^2$ ($k = 30$) to estimate the volume of ridged ice in the Arctic Ocean, while Leppäranta and Hakala (1992) obtained $k = 17$ in the Baltic Sea. The volume of ridged ice is typically 10–40% of total ice volume (Hibler *et al.*, 1974b; Mironov, 1987; Weeks, *et al.*, 1989; Lewis *et al.*, 1993; Granberg and Leppäranta, 1999).

Example In approximate terms, $b_R \approx 3h_k$ and $R \approx \sqrt{3}h_k^2$. Then $S_R/S \approx 5\mu h_k$ and $h_R \approx 3\mu h_k^2$. For representative values, taking $h_k \approx 7.5$ m and $\mu \approx 5\,\mathrm{km}^{-1}$, we have $S_R/S = 19\%$ and $h_R = 84$ cm. These numbers characterize a moderately ridged Arctic region.

In order to describe ridging properly, one needs at least three parameters: cut-off size, mean size, and ridge density. The cut-off size is a free parameter that needs to be "tuned" so that ridge statistics agree with the appearance of the ice field. These parameters can be used to obtain a ridging intensity measure, but the relationship cannot be inverted to obtain the ridge size and spacing from the intensity. However, there are regional regularities (Figure 2.24). In the central Arctic Ocean the size and density of ridges are correlated (Wadhams, 1981), while in the Weddell Sea the mean ridge size shows very small variations and could therefore be considered fixed (Granberg and Leppäranta, 1999). The latter case also holds in the Baltic Sea (Leppäranta, 1981b).

Example (Leppäranta, 1981b) In the Baltic Sea the average sail height is nearly constant, about 20 cm above the cut-off height of 40 cm. The ridge density alone provides a good estimator of the volume of ridged ice: in quantitative terms $h_R = 2.2\,\mathrm{cm}^2\mu \cdot 10^3 \pm 27\%$ (i.e., on average one ridge per kilometre accounts for 2.2 cm in ice thickness).

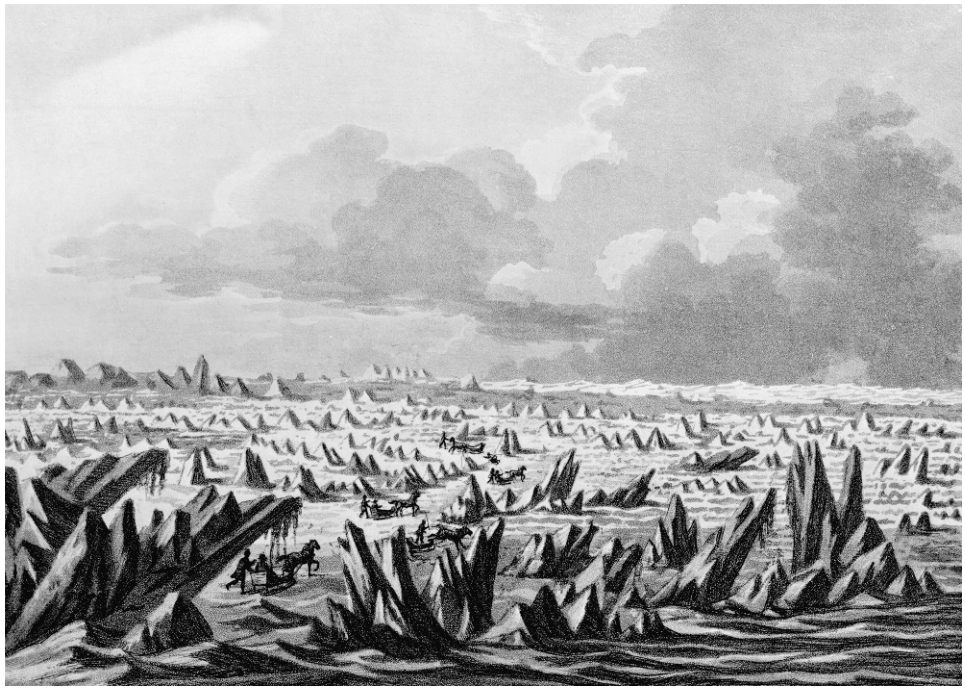

Figure 2.23 The Gulf of Bothnia in winter (Louis Belanger, according to A. F. Skjöldebrand). Travellers across a ridged ice field, a romantic drawing showing the ice landscape in exaggerated linear dimensions to create a fairy-tale atmosphere.
Reproduced from Etienne Bourgelin Vialart, comte de Saint-Morys, Voyage pittoresque de Scandinavie. Cahier de vingt-quatre vues, avec descriptions, 1802, with permission of Collections of Museovirasto, Helsinki, Finland.

2.5.4 Hummocked ice

Not all mechanically deformed ice appears as ridges: in places irregular, hummocked ice fields with no regular geometry are found. Their thickness is less than that of ridges but greater than that of undeformed, level ice. Their existence is well known to icebreaker captains, who consider them a nuisance because they may be hidden beneath the snow cover. Not many direct measurements exist about the spatial distribution of the thickness of hummocked ice. Such a field may be described by the mean and standard deviation of the thickness.

One way to estimate the volume of hummocked ice is to first consider the observation that the exponential distribution for ridge size holds for any manageable cut-off size. This suggests the following hypothesis: The exponential form can be extrapolated down to a zero cut-off height, but at some non-zero level the ridges lose their ridge-like form, which corresponds to the visual appearance of the ice field. The "ridges" beneath a well-chosen cut-off height are then taken to represent hummocked ice. Without any model for the geometry of hummocks, this extrapolation allows us to determine their total volume or the mean thickness h_h:

$$\frac{h_h}{h_h + h_R} = \frac{1}{2} \exp(-\lambda h_c)[1 + (\lambda h_c)^2] \tag{2.46}$$

In most ridge observations $\lambda h_c \sim \frac{1}{2}$, and therefore $h_h/(h_h + h_R) \sim \frac{1}{4}$. Knowing the volume of hummocks is enough for ice budget calculations but it would be desirable to decompose it into mean physical thickness and areal concentration. This would need a geometrical model of hummocked ice.

2.5.5 Total thickness of deformed ice

The mean thickness of deformed ice finally reads:

$$h_d = h_h + h_R \tag{2.47}$$

The spatial distribution of ridges has been traditionally described in terms of areal or volume fraction. Wittman and Schule (1966) reported that in the Canadian Basin the average areal fraction of pressure ice (equivalent to deformed ice) is 0.13–0.18 with a maximum of more than 0.5 in heavy-deformation zones, while according to Kirillov (1957) in the Kara Sea the average volume fraction is 0.28 with a maximum of 0.39.

The degree of ridging and hummocking has also been described by an index from 0 to 5. This index is roughly proportional to the total thickness of deformed ice, with full level 5 corresponding to $h_d/h_u \approx 1.5$–2.5, where h_u is the thickness of undeformed ice, and $h_i = h_u + h_d$ (Gudkovic and Romanov, 1976; Appel, 1989).

Example (*Kirillov's formula*) Kirillov (1957) made the following assumptions for ridges and hummocks: triangular sail and keel cross-sections and $h_k/h_s = 3$, on average $h_k = h_u$, and porosity equal to 0.3. Then $h_d/h_u \approx 2.0 \cdot S_R/S$. Thus observing the area of deformed ice provides an estimate for its volume.

2.6 DRIFT ICE STATE

In the continuum dynamics of sea ice, an ice state J must be defined. It is the set of the material properties of drift ice necessary to solve the dynamics problem. When the number of properties included in J is N we speak of an N-level ice state. Most work in continuum sea ice dynamics has been done by assuming that the ice thickness field is sufficient to describe the state of drift ice. In practice, there are observational limitations to map the thickness field as discussed in Section 2.4.

The first approach is to define ice categories as the ice state variables. Normally these are chosen to be manageable observables, meaning that the ice state is largely based on the information provided by routine ice mapping systems. Recall the function "ice", I, from Eq. (2.4). In a low-level approach it is necessary to define generalized compactness and mean thickness of ice:

$$A(h_0) = \frac{1}{S}\int_\Omega I(x, y; h_0)\, d\Omega \tag{2.48a}$$

$$\tilde{h}(h_0) = \frac{1}{S}\int_\Omega hI(x, y; h_0)\, d\Omega = A(h_0)\tilde{h}_i(h_0) \tag{2.48b}$$

where $\tilde{h}_i(h_0)$ is the mean ice floe thickness over the sub-region $\Omega \cap \{h > h_0\}$. These quantities thus account for all ice thicker than h_0. Very thin ice does not give significant resistance to deformation, and it is preferable to exclude it from the mean thickness for the strength estimator. On the other hand, in remote sensing very thin ice is not well detected, and consequently $A(h_0)$ corresponds better to initialization and validation data. The areal fraction $1 - A(h_0)$ is the concentration of open water and thin ice; ice only grows there thermodynamically. The argument h_0 is no longer shown below but any category may be chosen conditional on $h > h_0$.

Compactness or mean thickness would be natural one-level ice states but they are not used because of too limited information. The minimum feasible ice state is their union, which is in fact the very widely used *two-level ice state* (Nikiforov, 1957; Doronin, 1970):

$$J = \{A, \tilde{h}\} \tag{2.49}$$

or, since $\tilde{h} = A\tilde{h}_i$, the state $J = \{A, \tilde{h}_i\}$ has the same information.

For *three-level ice states*, the decomposition of ice into undeformed ice and deformed ice (Leppäranta, 1981a) is often used:

$$J = \{A, h_u, h_d\} \tag{2.50}$$

The thickness of undeformed ice changes thermodynamically, while undeformed ice is dynamically transformed into deformed ice. This state does not include the areas of undeformed ice and deformed ice, just their thicknesses, and formally accounting for the area also would not be difficult. Lu *et al.* (1989) used another three-level system: ice compactness, first-year ice, and multi-year ice. The timescale was less than 1 month, and therefore these ice categories were independent but very useful

for modelling dynamics because of their different thicknesses and observability. Mechanical deformation may then be correctly limited to first-year ice only.

The ice category approach can be extended to multi-level ice states $J = \{A, j_1, j_2, j_3, \dots\}$. Additional, reasonable, new ice categories are introduced based on their dynamical significance and observability (Haapala, 2000). With a morphological model, more information can be extracted from one category. Leppäranta (1981a) decomposed deformed ice into density and size of ridges, these being controlled visually or with a laser profilometer.

The second approach is to take the *thickness distribution* for the ice state. The question then becomes: How many levels are needed or, in other words, what is the necessary or convenient resolution of the distribution? The thickness classes are fixed, arbitrarily spaced, and their histogram contains the state variables:

$$J = \{\pi_0, \pi_1, \pi_2, \dots, \pi_N\}, \quad \sum_{k=0}^{N} \pi_k = 1 \tag{2.51}$$

The open water fraction is practically always needed and therefore $\pi_0 = 1 - A$ or in general $\pi_0 = 1 - A(h_0)$.

In low-level cases thickness distribution approach is a very crude system in which the actual ice thickness information can easily disappear. Hence, the approach based on ice categories is preferable. The two-level state based on the thickness distribution is not the same as the two-level state based on the ice categories, since in the former case the thickness (or rather the thickness band) is fixed. In new, growing ice, it would need to spread evenly all over the ice band, far from what really happens. Consequently, when choosing the thickness distribution for the ice state the number of thickness classes should be large (of the order of ten). For such a number of levels, the ice category approach becomes cumbersome and the thickness distribution approach becomes preferable.

Example If there are no thermodynamical changes and mechanical changes only concern ice compactness, the two-level ice category and thickness distribution approaches overlap. The former is $J = \{A, \tilde{h} = \text{constant}\}$ and the latter is $J = \{\pi_0, \pi_1 = 1 - \pi_0\}$ (i.e. only $\pi_0 = 1 - A$ and A change).

Also, a combination can be worked out to add more observability to the thickness distribution. One possibility is to divide the thickness distribution into two parts: undeformed and deformed ice. This would allow us to differentiate thermal ice growth from mechanical ice growth.

In principle, the horizontal properties of ice floes can be added to the ice state in a similar way to thickness. Floes possess size and form, and size at least shows statistical regularity (see Section 2.2). In the continuum dynamics of sea ice, floe information has been used only in floe collision models (Shen *et al.*, 1986), there taken as uniform, circular disks. However, when an ice field closes up floes join together to act in groups and their individual signature is lost out from mechanical behaviour of the ice field. Application of discrete particle models to ice mechanics necessitates the detailed knowledge of the size and shape of all ice floes in the study area.

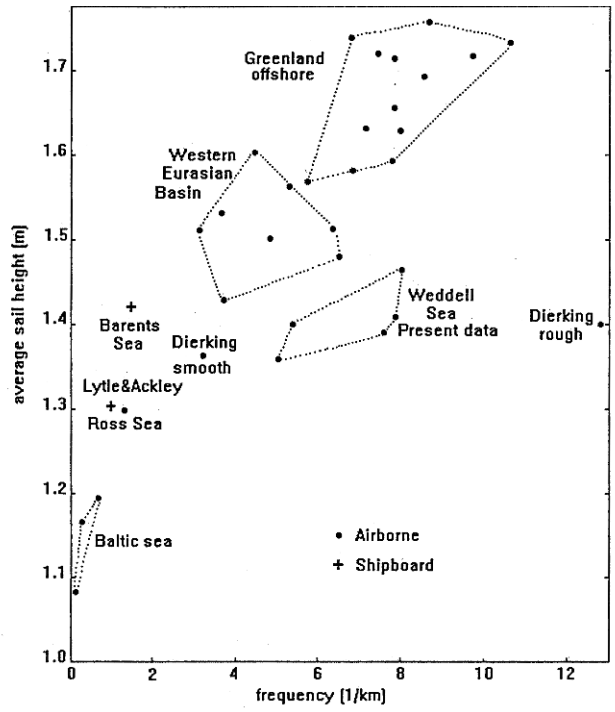

Figure 2.24 Ridge sail height vs. ridge density in different seas. Cutoff is 1 m.
From Dierking (1995), Granberg and Leppäranta (1999), Lytle and Ackley (1991), and Wadhams (1981).

Beginning with sea ice in the world ocean, sea ice types, and sea ice observation systems, the geophysical medium of drift ice has been introduced in this chapter. The drift ice medium appears as a thin, broken film on the sea surface, almost truly 2-dimensional. It consists of ice floes and is regarded as a continuum over length scales much greater than the typical size of floes. The relevant properties of the drift ice continuum for its dynamics are mainly ice compactness and thickness, which vary largely in time and space. The last section presented the concept of an "ice state", which contains information about the drift ice field necessary to understand and model its dynamics. In Chapter 3 observations about the kinematical properties of the drift ice medium are presented.

http://www.springer.com/978-3-642-04682-7

The Drift of Sea Ice
Leppäranta, M.
2011, XXX, 350 p., Hardcover
ISBN: 978-3-642-04682-7